J. Fluid Mech. (1997), *vol.* 335, *pp.* 75–109

Collision statistics in an isotropic particle-laden turbulent suspension. Part 1. Direct numerical simulations

By SHIVSHANKAR SUNDARAM AND LANCE R. COLLINS

Department of Chemical Engineering, The Pennsylvania State University University Park, PA 16802, USA

(Received 1 December 1995 and in revised form 1 October 1996)

Direct numerical simulations of heavy particles suspended in a turbulent fluid are performed to study the rate of inter-particle collisions as a function of the turbulence parameters and particle properties. The particle volume fractions are kept small ($\sim 10^{-4}$) so that the system is well within the dilute limit. The fluid velocities are updated using a pseudo-spectral algorithm while the particle forces are approximated by Stokes drag. One unique aspect of the present simulations is that the particles have finite volumes (as opposed to point masses) and therefore particle collisions must be accounted for. The collision frequency is monitored over several eddy turnover times. It is found that particles with small Stokes numbers behave similarly to the prediction of Saffman & Turner (1956). On the other hand, particles with very large Stokes numbers have collision frequencies similar to kinetic theory (Abrahamson 1975). For intermediate Stokes numbers, the behaviour is complicated by two effects: (i) particles tend to collect in regions of low vorticity (high strain) due to a centrifugal effect (preferential concentration); (ii) particle pairs are less strongly correlated with each other, resulting in an increase in their relative velocity. Both effects tend to increase collision rates, however the scalings of the two effects are different, leading to the observed complex behaviour. An explanation for the entire range of Stokes numbers can be found by considering the relationship between the collision frequency and two statistical properties of the particle phase: the radial distribution function and the relative velocity probability density function. Statistical analysis of the data, in the context of this relationship, confirms the relationship and provides a quantitative description of how preferential concentration and particle decorrelation ultimately affect the collision frequency.

1. Introduction

Collision and coagulation processes of particles suspended in turbulence are of considerable significance in a wide variety of both natural and industrial flows. Raindrop growth in the atmosphere, aerosol processing, pneumatic transport of solids are only a few examples. Typically, one needs to calculate particle growth rates in a given flow and understand the effect of various particle and fluid parameters on these growth rates. The rate at which particles are brought in contact or the collision frequency is the critical quantity required to model the evolution of such particle systems.

Traditionally, coagulation processes have been separated into distinct macrophysical and microphysical problems. The microphysical problem involves the computation of rates of particle encounters and their dependence on parameters that characterize these flows. The macrophysical aspect, then, involves using these generated collision frequencies and a population model to arrive at the evolution of the particle size distribution as a function of time. In this study, we shall be concerned solely with the microphysical problem of collision rates of particles in turbulent flow.

Particle encounters are extremely difficult to observe experimentally, even given today's sophisticated laser measurements. The advantage of numerical simulations, on the other hand, lies in the wealth of detailed information on particle and fluid motion. Detection and implementation of particle interactions in a simulation, while posing a considerable numerical challenge, introduces no fundamental difficulties. In this context, information from numerical simulations on collision frequencies is vital in validating any theoretical effort in describing the microphysical problem.

Direct numerical simulation is a means of numerically integrating the full Navier–Stokes equations governing fluid motion without resorting to any *ad-hoc* modelling. Over the last two decades such simulations have gained wide acceptance as an important source of information on various dynamical aspects of turbulence. Computing the motion of particles in these flows, under prescribed interaction laws, is straightforward. Consequently, particulate turbulent flows have also been the subject of numerous investigations in the past. The first numerical simulation of particles suspended in turbulence was performed by Riley & Paterson (1974). This and many later studies (Yeung & Pope 1988; Squires & Eaton 1990; Elghobashi & Truesdell 1992 to mention a few) were devoted to understanding the phenomenon of particle dispersion by turbulence. The limited resolution or scale separation of earlier studies was not a severe drawback in view of the dominant role played by the well-resolved large eddies in diffusion of suspended particles. With the explosive growth in computational power, modern simulations are able to better resolve an adequate range of small-scale motion, providing the ability to analyse a host of new problems. Thus, more recent efforts were focused on small-scale-driven phenomena such as the modification of turbulence by particles (Squires & Eaton 1990; Elghobashi & Truesdell 1993) and spatial structure of particle concentration fields (Squires & Eaton 1991; Wang & Maxey 1993). These studies involved tracking anywhere from 10^4 to 10^6 particles in order to observe statistically significant effects of the particles. Additionally, investigations of aerosol particle trapping and deposition have been performed in boundary layer flows (Kallio & Reeks 1989) and channel flows (Mclaughlin 1989; Brooke *et al.* 1992; Brooke, Hanratty & McLaughlin 1994). These studies also neglect particle collisions and only assume a particle size for the purpose of determining deposition rates.

Most computational processes involving particle updates (including checking for wall collisions) are $O(N_p)$, where N_p is the total number of particles in the system. However, detection of particle collisions involves sorting through all particle pairs and hence is $O(N_p^2)$. This aspect of the simulation can easily swamp the rest of the calculation. As a result, all of the previous studies implemented 'point' particles with no direct particle interactions. However, the finite size of particles can play a very significant role in turbulence modulation, preferential concentration and other so-called 'particle effects' (Sundaram & Collins 1994*a, b*). Upon considering finite-volume particles, the issue of particle collisions immediately becomes central to the simulation. Sundaram & Collins (1996) adapted techniques in the molecular dynamics literature to render computation of such finite-volume particles in turbulence, with collisions, feasible. The main idea was to examine only a relatively small neighbourhood (rather

than the entire computational volume) surrounding a particle to detect collisional partners. Thus, the motion of *finite* size particles responding to turbulent fluctuations and direct impact is simulated, allowing us to quantify the rate of particle collisions and the role of turbulence in bringing these particles into contact.

At this stage, it is worth noting the major assumptions that are made in the simulations. First, it is assumed that the principal interaction between the fluid and particle phases is represented by the Stokes drag term, which can be shown to be of leading order in the limit of small Stokes number (Maxey & Riley 1983). Second, the particle inertia (quantified by the particle Stokes number) is assumed to be sufficient to allow particle contact when particle trajectories cross. The effect of the lubrication layer between particles near contact is entirely neglected in this analysis. It is recognized that the lubrication layer can strongly influence the so-called *collision efficiency* in real aerosols (Jonas & Goldsmith 1972). As a result, the definition of 'collision frequency' in the present study should be thought of as an 'arrival rate'. The determination of whether an arrival will lead to a true collision requires a detailed analysis of the lubrication layer. The reader may refer to recent results that show promise in quantifying these processes (Sundararajakumar & Koch 1996). Finally, the simulations are restricted to isotropic turbulence and gravity is neglected for the sake of simplicity.

Collisional growth of colloidal particles in aqueous media has been a problem of practical and theoretical interest since the turn of the century. These particles may coagulate under some or all of hydrodynamic, gravitational, Brownian, electrostatic and thermal (Marangoni) forces. Significant work has been done in the area of flow-induced coagulation at low Reynolds numbers. Treatment of particle motion is simplified by the creeping flow assumption where the particle motion can be treated as a superposition of independent hydrodynamic, Brownian and other motions. The first attempt at treatment of a simple shear-induced coagulating system was made by Smoluchowski (1917). In his analysis he neglected any particle hydrodynamic interaction other than a sticking force on contact and arrived at the conclusion that collisions were directly proportional to the laminar shear rate. Curtis & Hocking (1970) included hydrodynamic interactions between the particles undergoing collision and coagulation in a shear flow. Hocking & Jonas (1970) calculated collision and coagulation rates in a system of sedimenting spherical particles using Stokesian theory. To allow particle coalescence in the presence of lubrication forces, they introduced a parameter whereby coalescence was assumed if the inter-particle distance was less than a prescribed fraction of particle diameter. More recently, sophisticated techniques like trajectory analysis (Zeichner & Schowalter 1977; Davis 1984) and solution of the pair distribution function equation (Wen & Batchelor 1985) have been brought to bear on the problem of coagulating spherical particles. Many of these analyses rely on the Stokesian flow assumption which enables the use of the general solution for motion of two spheres under creeping flow conditions (Batchelor & Green 1972). The absence of any similar formalism for particle pair motion in turbulent flow renders the extension of such approaches to calculating collision frequencies in turbulent flows infeasible. Related studies at the present time involve extension of similar techniques to droplet collisions in simple external flows, a problem complicated by the presence of internal circulation (Wang, Zinchenko & Davis 1994).

Turbulence controls particle motion by means of the fluctuating drag force. Apart from dictating particle velocity distributions, in the presence of finite particle inertia this interaction also causes non-uniform particle spatial distributions (as will be shown). Collisions are driven solely by relative motion between particles. Local turbulence fluctuations affect particle encounters by contributing to relative motion

of neighbouring particles. In the absence of any other force creating relative motion between particles, these local fluctuations entirely control relative velocity distribution. Saffman & Turner (1956) performed a pioneering analysis of the problem of polydisperse raindrop growth in atmospheric turbulence. In the limit of particles smaller than the smallest turbulence scales, they surmised that the relative velocity between particles scaled as the local velocity gradient over the particle diameter. They obtained a collision frequency of particles in turbulence independent of particle properties (discussed in the next section). As a consequence of zero inertia, spatial non-uniformities are not taken into account in their formulation. Their result can be viewed as a limiting analysis valid for finite-sized fluid tracers in turbulent flow. Abrahamson (1975) extended concepts from kinetic theory of gases in an effort to incorporate the influence of particle inertia. Once again, particle accumulation was not considered. Our goal, in this study, is to systematically investigate the influence of particle parameters (specifically inertia) on collision frequencies in a turbulent particle-laden suspension.

The paper is organized as follows: §2 outlines essential details of the theory of flow-driven collisions in particulate suspensions. The governing equations and the numerical methods used are set out in §3. Results from the simulations are discussed in §4. Section 5 compares the statistical expression for collision frequency derived in §2 with the simulation results, followed by conclusions in §6.

2. Theory

Consider a system of N_p particles of diameter σ in a volume V. From a development analogous to kinetic theory of gases (see the Appendix for details) we can represent the collision frequency in such a monodisperse particulate system as

$$N_c = \tfrac{1}{2}\pi\sigma^2 n^2 \int w P^{(2)}(\boldsymbol{w}, \sigma)\ \mathrm{d}\boldsymbol{w} \tag{2.1}$$

where n is the particle number density, $\boldsymbol{w}$ is the relative velocity between two particles and $P^{(2)}(\boldsymbol{w}, \sigma)$ is the particle pair probability distribution which can be interpreted as follows: $P^{(2)}(\boldsymbol{w}, \boldsymbol{r})\ \mathrm{d}\boldsymbol{w}\mathrm{d}\boldsymbol{r}$ is the fraction of pairs of particles located in a volume between $\boldsymbol{r}$ and $\boldsymbol{r} + \mathrm{d}\boldsymbol{r}$ with relative velocity between $\boldsymbol{w}$ and $\boldsymbol{w} + \mathrm{d}\boldsymbol{w}$. Separating the pair distribution into distinct spatial and velocity distributions, we obtain

$$N_c = \tfrac{1}{2}\pi\sigma^2 n^2 g(\sigma) \int w\ P(\boldsymbol{w}|\sigma)\ \mathrm{d}\boldsymbol{w} \tag{2.2}$$

where $P(\boldsymbol{w}|\sigma)$ is the *conditional* relative velocity probability density function at contact and $g(\sigma)$ is the particle radial distribution function (RDF) at contact. This is an intuitively reasonable result based on the following arguments. Collisions involve the presence of two particles and hence the rate of particle collisions is expected to be proportional to the number density squared. Spherical particles of diameter σ present an effective cross-section proportional to the square of the diameter. The fact that particles with greater relative velocity will collide more often is reflected in the first moment of the relative velocity distribution. The radial distribution function term, $g(\sigma)$, is a correction to the local number density due to non-uniform particle spatial distribution. The factor of $1/2$ is introduced to avoid double counting of collisions between identical particles.

Particle collision in turbulence lends itself to analytical treatment in the limits of particle motion being completely controlled by turbulence (zero inertia – Saffman–

Turner limit) and particles being completely uncorrelated with the fluid and with each other (infinite inertia – kinetic limit). Equation (2.2) can be treated as the starting point in the derivation of both limiting expressions. As mentioned before, the Saffman–Turner result follows from approximating the relative velocity distribution as a Gaussian with variance specified as follows:

$$\mathrm{Var}(\boldsymbol{w}) = s^2 = \frac{1}{5}\left(\frac{\sigma}{\tau_\eta}\right)^2; \tag{2.3}$$

$\tau_\eta \equiv (\nu/\epsilon)^{1/2}$ is the smallest turbulence timescale determined by the kinematic viscosity ν and the turbulent dissipation ϵ. As particle positions are random in the absence of inertia and the particle volume fraction is small, $g(r) \approx 1$. Substituting in (2.2) we obtain

$$N_c = \tfrac{1}{2}\pi\sigma^2 n^2 \int w \left(\frac{3}{2\pi s^2}\right)^{3/2} \exp\left(-\frac{3w^2}{2s^2}\right) \mathrm{d}\boldsymbol{w}$$

Carrying out the integration,

$$N_c = \tfrac{1}{2}n^2\sigma^2(8\pi s^2/3)^{1/2} = \tfrac{1}{2}n^2\sigma^2\left(8\pi\frac{1}{15}\left(\frac{\sigma}{\tau_\eta}\right)^2\right)^{1/2}.$$

Upon simplification the Saffman expression for the collision frequency in a particulate turbulent system is obtained:

$$N_c = \tfrac{1}{2}n^2\sigma^3\left(\frac{8\pi}{15}\frac{\epsilon}{\nu}\right)^2. \tag{2.4}$$

Notice that the collision frequency, as stated, depends only on particle size and concentration apart from fluid dissipation and viscosity.

Next, we consider the limit of particles with very large inertia. In this limit, the particles are assumed to be randomly positioned with independent velocities that are characterized by a Maxwellian distribution. For two neighbouring particles with Maxwellian velocity distributions it can be easily shown that the relative velocity too is Maxwellian. This can be seen by considering the variance of the *relative velocity*:

$$\mathrm{Var}(\boldsymbol{w}) = \mathrm{Var}(\boldsymbol{v}_1 - \boldsymbol{v}_2) = \mathrm{Var}(\boldsymbol{v}_1) + \mathrm{Var}(\boldsymbol{v}_2) - 2\mathrm{Cov}(\boldsymbol{v}_1, \boldsymbol{v}_2) \tag{2.5}$$

Since the particles are assumed independent of each other the covariance is identically zero and given that the particles are sampled from the same distribution

$$\mathrm{Var}(\boldsymbol{w}) = 2\mathrm{Var}(\boldsymbol{v}) = 2\overline{v_p^2}. \tag{2.6}$$

Again, due to the assumption of a spatially homogeneous particle concentration field and small particle volume fraction, $g(r) \approx 1$ for $r > \sigma$. Representing the variance of the velocity distribution by $\overline{v_p^2}$ and carrying out the integrations as before gives

$$N_c = \tfrac{1}{2}n^2\sigma^2\left(\frac{16\pi\overline{v_p^2}}{3}\right)^{1/2}. \tag{2.7}$$

This result was also obtained by Abrahamson (1975). In contrast to (2.4), the collision frequency (in this limit of random, uncorrelated particles) is proportional to the square root of the energy contained in the particulate phase.

The motion of particles with finite inertia is decidedly more complicated than either of the two limits discussed above. The complication arises from two distinct effects,

both of which strongly influence the particle collision frequency: (i) particles with finite inertia tend to accumulate in regions of low vorticity (high strain) due to a centrifugal effect, resulting in inhomogeneities in the particle concentration field (referred to as preferential concentration) and (ii) relative motion between neighbouring particles is now generated by a combination of correlated and uncorrelated motions. Effect (i) increases the collision frequency, while effect (ii) can increase or decrease the collision frequency depending on the value of the Stokes number.

It should be noted that preferential concentration of particles vanishes in the Stokes number limits $St \to 0$ and $St \to \infty$. Furthermore, in these limits, the relative velocities between neighbouring particles are completely characterized by a single parameter (ϵ and $\overline{v_p^2}$, respectively), which explains why simple analytical expressions for the collision frequency exist in these two limits. Unfortunately, the description of collision frequencies at intermediate Stokes numbers is contaminated by preferential concentration and the complex mechanism responsible for relative motion between particles. Moreover, the dynamics in the intermediate regime does not resemble either of the two limits, but rather is qualitatively changed by the combination of the two effects.

Understanding relative motion of finite-inertia particles at intermediate Stokes numbers and the influence of various particle and fluid parameters on that motion is, perhaps, the single most significant step required to understand collisions in a particle-laden turbulent flow field. While the relative velocity distributions can be profitably assumed to be exponential or Gaussian in the limit of zero and infinite inertia respectively, extension of similar thinking to intermediate-Stokes-number particles still needs to be validated. Adjacent spatial fluid structures, such as co-rotating vortices, coupled with the particles tendency to 'remember' their velocity history could induce longer tails in the relative velocity distribution than prescribed by either distribution. Thus, while it is clear that the variance in relative velocities will increase with increasing particle inertia (not without limit, as will be seen later), the exact form of its distribution is not evident.

In addition, we must quantify the degree to which preferential concentration affects particle collision frequencies. Local number densities an order of magnitude higher than the average have been observed in this study and elsewhere (Squires & Eaton 1991; Wang & Maxey 1993). The effect this has on the RDF at contact (the quantity used in the collision formula, (2.2)) must be determined from the simulations.

3. Governing equations and numerical solution

3.1. *Particle phase*

This study is restricted to solid, spherical particles (no internal flow) of much greater density than the suspending fluid, smaller than the smallest scales of flow (i.e. Kolmogorov scale, η) but larger than the molecular mean free path (λ) of the fluid so that Brownian motion due to bombardment by fluid molecules may be neglected ($Pe \to \infty$). While appearing severely restrictive, these assumptions are valid for a wide variety of natural (e.g. raindrops in atmospheric turbulence) and industrial processes. Additionally, we are neglecting gravitational forces to simplify the interpretation by preserving the isotropic nature of the particle velocity field.

3.1.1. *Governing equations for particles*

Under the assumptions that $\sigma/\eta < 1$ and $Re_p = \sigma|u - v_p|\nu_f < 1$, Maxey & Riley (1983) derived the equation of motion for a particle suspended in turbulent flow. For

dense particles, it can be shown that the the drag force is of leading order. Including particle–particle direct interactions via hard-sphere collisions, the complete equation of motion for the ith particle can be specified as

$$\frac{\mathrm{d}\boldsymbol{v}_{p_i}}{\mathrm{d}t} = \frac{\boldsymbol{u}(\boldsymbol{X}_{p_i}) - \boldsymbol{v}_{p_i}}{\tau_p} + \frac{1}{m_p}\sum_{j\neq i} F_{ij}, \tag{3.1a}$$

$$\frac{\mathrm{d}\boldsymbol{X}_{p_i}}{\mathrm{d}t} = \boldsymbol{v}_{p_i} \tag{3.1b}$$

where m_p is the mass of a single particle, $\boldsymbol{u}(\boldsymbol{X}_p)$ is the fluid velocity at the particle centre and F_{ij} is the instantaneous force due to a perfectly elastic collision (in this context, elastic refers to conservation of initial momentum and energy). Note the appearance of the the particle response time defined as $\tau_p = \rho_p\sigma^2/18\mu$ which is a measure of the particle inertia. Dimensionless forms of particle properties such as diameter and response time can be obtained by taking their ratio with suitable fluid scales. Given that turbulence is a multi-scaled phenomenon, the choice of normalizing scales is not obvious. However, considering that we are interested in particles smaller than the smallest turbulence scales we choose to normalize using the Kolmogorov scales. This is in contrast to investigations of large-eddy-controlled particle behaviour, such as particle dispersion, where normalization by the integral scales is more relevant. A particle Stokes number can then be defined as

$$St = \frac{\tau_p}{\tau_\eta} = \frac{\epsilon^{1/2}\tau_p}{\nu^{1/2}} \tag{3.2}$$

The limit $St = 0$ indicates a fluid tracer while $St = \infty$ denotes a heavy particle completely unresponsive to the flow.

The assumption of linear drag is valid under the condition $Re_p < 1$. In view of the low particle Reynolds numbers encountered, inclusion of nonlinear drag was deemed unnecessary. Looking at (3.1) it can be seen that fluid velocities along the as yet undetermined particle paths are required to solve for the particle motion. This coupling renders the system complicated to solve. In fact this relatively simple-looking equation has no closed-form analytic solution. A maximum of 64^3 particles was tracked to obtain the collision statistics presented in the study. This number was found to be sufficient to generate satisfactory statistics.

3.1.2. *Fluid interpolation*

The requirement of fluid velocities at particle centres necessitates some form of interpolation of the fluid grid velocities onto particle locations. The presence of a spectral representation of the fluid velocities suggests the use of spectral interpolation, but this involves $O(N^3)$ operations per particle and is prohibitively expensive. However, advantage can be taken of the availability of spectral representation in that velocity derivatives at grid points can be calculated accurately. It has been demonstrated in recent papers (Yeung & Pope 1988; Balachandar & Maxey 1989) that a minimum of third-order spatial accuracy is needed to resolve the particle motion. Accordingly, we used a cubic Hermite spline interpolation function which uses the value of the velocity and its derivatives at the corners of the cube surrounding the particle. An accompanying study (Sundaram & Collins 1996) demonstrated the lack of any significant dependence of collision frequencies on the order of the interpolation function used. The particle velocities are then updated using a second-order Runge–Kutta method.

3.1.3. *Collisions*

The novel aspect in this study is the inclusion of particle interactions through hard-sphere elastic collisions. A brief summary of the algorithm used for detecting and implementing particle collisions will be provided here. However, the interested reader is referred to Sundaram & Collins (1996) for additional details. Calculating particle–particle encounters involves $O(N_p^2)$ operations and considering the numbers of particles needed for smooth statistics is clearly infeasible. However, recognizing that particle collisions are strictly a local phenomenon involving particles that are in the neighbourhood of a given particle, one can effect a substantial reduction in the computational cost involved in detecting collisions. Similar to Pearson, Valioulis & List (1984), we employ an efficient neighbourhood search algorithm which first groups particles into non-overlapping cells. Subsequently, for any given particle, the algorithm searches through the cell containing the particle and the surrounding cells to identify particle encounters within a time step. The computational savings are proportional to the ratio of the cell volume examined to the total volume of the system, i.e. $O(l/L)^3$ where l is the cell size and L is the system size. The optimal cell size l depends on parameters such as particle velocities and the time interval considered. Upon consideration of the constraint that, over the particle update time interval Δt, all collision partners for a given particle must be contained within the cells searched, a condition on the minimum cell size is obtained:

$$\frac{v_p^{max}\Delta t}{l} < 1$$

where v_p^{max} is the maximum particle velocity. Once identified, particle collisions are enacted in the time order in which they occur. This implementation inherently restricts us to a first-order particle position time advancement.

To validate our collision routines we simulated a fluid–free particle system with Maxwellian initial velocity distribution and random non-overlapping initial positions. The system then evolves under the rules of momentum- and energy-preserving hard-sphere collisions. This system is completely characterized by the number density of particles n, diameter of particles σ and the energy content in the system $\overline{v_p^2}$. The energy content is directly analogous to the specification of a temperature in a monodisperse gas:

$$\tfrac{1}{2}\overline{v_p^2} = \frac{3}{2}\frac{KT}{m_p}.$$

Indeed, as mentioned earlier, this provides a convenient reference point for interpreting results from suspended particles. The particle collision frequency for such a system can be calculated from principles of kinetic theory and is given by (2.7). Figure 1(*a*) shows the excellent agreement between calculated and simulated values of the collision frequency. The slight discrepancy can be attributed to the finite volume occupied by the particles. Moreover, analytical results are available for the distribution of the velocity and relative velocity magnitudes of colliding particles. The agreement between numerical and analytical results for the velocity distribution functions as shown in figures 1(*b*) and 1(*c*) are further confirmation of the accuracy of the collision procedures.

3.2. *Fluid phase*

The fluid phase in this study is governed by the incompressible Navier–Stokes equations.

$$\nabla \cdot \boldsymbol{u} = 0, \tag{3.3a}$$

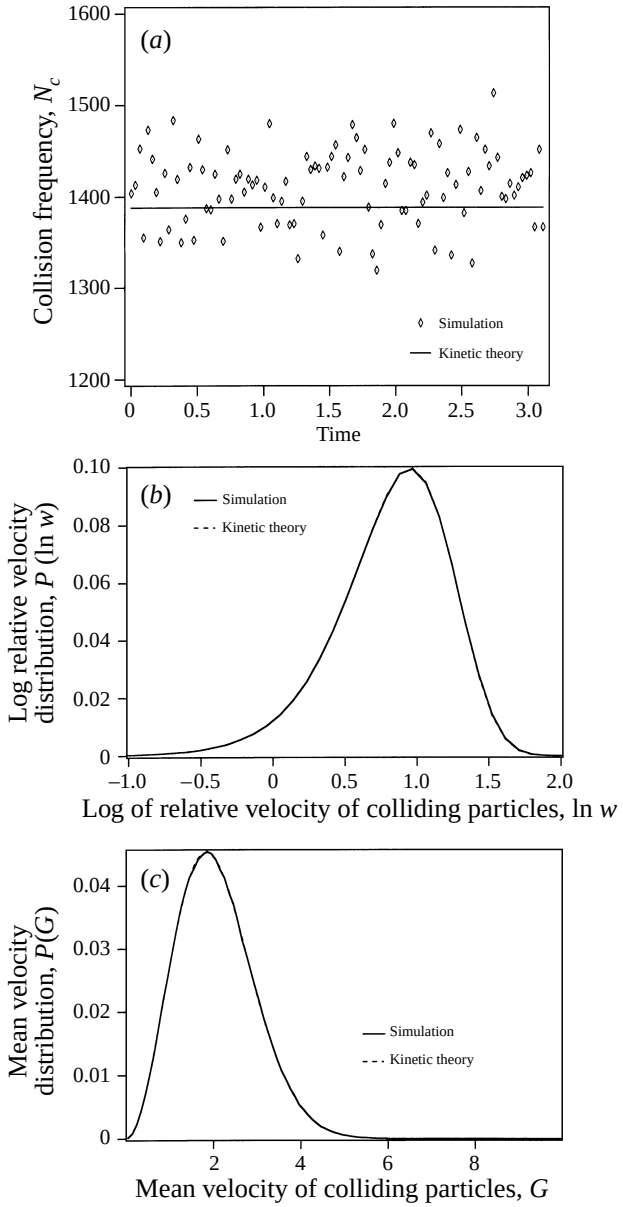

FIGURE 1. (*a*) Comparison of collision frequencies observed in a fluid–free particle system initialized with a Maxwellian velocity distribution and the analytical result from kinetic theory (2.7). (*b*) Comparison of velocity distributions of colliding particles for the test system with analytical result from kinetic theory. (*c*) Comparison of *relative* velocity distributions of colliding particles for the test system with analytical result from kinetic theory.

$$\frac{\partial \boldsymbol{u}}{\partial t} + \boldsymbol{u} \cdot \nabla \boldsymbol{u} = -\frac{1}{\rho_f} \nabla P + \nu \nabla^2 \boldsymbol{u} + \boldsymbol{F}_t \tag{3.3b}$$

Here $\boldsymbol{u}(\boldsymbol{x}, t)$ represents a three-dimensional time- and space-varying velocity field, ρ_f is the density of the fluid and $P(\boldsymbol{x}, t)$ is the pressure field. Turbulence, left without any means of energy input, will decay. This introduces additional complications in

the form of time-evolving scales of motion. Hence, for ease of interpretation, it was decided to force the turbulence so that the flow field will remain stationary in time. This requires an energy input, specified as the forcing function $\boldsymbol{F}_t$ in (3.3*b*) and described in detail below, which has to satisfy certain constraints in order to preserve the random and isotropic nature of the turbulence.

It should be noted that in the equations as presented in (3.3*b*), there is no influence of the particles on the fluid (i.e. no reverse coupling). The presence of particulates, or any other phase for that matter, modifies the Navier–Stokes equations for the fluid in two ways – firstly, the non-zero volume occupied by the secondary phase changes the continuity equation and secondly phase interactions introduce an exchange term in the fluid momentum equation. At the extremely low particle volume loadings that we consider ($\sim O(10^{-4})$), the direct influence of the volume occupied by particles on the continuity equation can be neglected. However, although the particle volume fractions are low, the influence of the particle phase on the fluid kinetic energy can be significant on account of the higher particle mass loading. We have chosen to neglect this effect in this study so that we can study the dynamics of the particle field suspended in a fluid flow field that is identical from run to run. The Navier–Stokes equations are discretized on a cubic domain of length 2π using N^3 grid points. Periodic boundary conditions are imposed as for the particles. Wavenumbers are then correspondingly defined by

$$k_i = i, \qquad i = 0, \ldots, N/2. \tag{3.4}$$

The maximum possible wavenumber, $N/2$, is denoted by k_{max}. There is no mean flow. The fluid is then updated using a pseudo-spectral algorithm similar to the one described in Canuto *et al.* (1988). Partial dealiasing is accomplished by zeroing wavenumbers beyond $\frac{8}{9}k_{max}$ as originally suggested by Patterson & Orzsag (1972). Time advancement is done using an efficient fourth-order Runge–Kutta scheme.

The grid resolution for the fluid calculation was set at $N = 64$ after many considerations. Particle tracking with collision detection takes up a substantial portion of the available computational resources, effectively prohibiting any higher resolution of the fluid phase. While higher resolutions would exhibit a better separation of scales and a longer inertial range, it must be recalled that this study is concerned with sub-Kolmogorov-scale particles where the important fluid phenomena controlling particle motion are expected to occur at the small scales. The dissipation-range dynamics are as well represented at this resolution as in any higher ones. Higher resolutions can then mainly contribute in resolving the question of the influence of asymptotically large Reynolds numbers.

Important fluid properties and scales are summarized in table 1. The turbulent intensity, u', and dissipation rate, ϵ, are obtained from the energy spectrum, $E(k)$, as

$$\tfrac{3}{2}u'^2 = \tfrac{1}{2}q^2 \equiv \int_0^{k_{max}} E(k)\,\mathrm{d}k$$

$$\epsilon \equiv 2\nu \int_0^{k_{max}} k^2 E(k)\,\mathrm{d}k$$

where ν is the fluid kinematic viscosity. The integral length scale, L_f, is obtained as

$$L_f = \frac{\pi}{2u'^2} \int_0^{k_{max}} \frac{E(k)}{k}\,\mathrm{d}k$$

Parameter	Value	Parameter	Value
u'	1.0898	τ_k	0.242
ϵ	0.2145	λ	0.799
ν	0.0126	Re_λ	54.2
L_f	1.646	$k_{max}\eta$	1.77
T_e	1.932	Δt	0.0031
η	0.0552		

TABLE 1. Listing of parameters needed to describe the fluid-phase turbulence. Additionally, the length and time scales of the flow are listed for easy reference.

with the associated integral timescale, T_e, defined as

$$T_e \equiv L_f/u'.$$

The Kolmogorov length and time scales, η and τ_k, are given by

$$\eta \equiv \left(\frac{\nu^3}{\epsilon}\right)^{1/4}$$

and

$$\tau_k \equiv \left(\frac{\nu}{\epsilon}\right)^{1/2}.$$

The Taylor microscale, λ, was obtained using

$$\lambda \equiv \left(\frac{15\nu u'^2}{\epsilon}\right)^{1/2}$$

The Reynolds number listed in the table, Re_λ, is calculated as

$$Re_\lambda \equiv \frac{u'\lambda}{\nu}.$$

It is widely accepted that the product $k_{max}\eta$ should be greater than unity for good resolution of the small scales. Its value in our simulation along with the time step Δt are also provided in table 1. The spatial energy and dissipation spectra from the simulations, normalized by their single point values, are shown in figure 2. These were obtained by averaging the spectra calculated over six eddy turnover times sampled once every half eddy turnover time. The peaking of the dissipation spectrum well before $k\eta \approx 1$ is confirmation that the small or dissipative scales are well resolved.

As mentioned before, energy is added to the system to force the flow to remain statistically stationary in time. Following Eswaran & Pope (1988), this forcing is accomplished by means of a complex, vector-valued Ornstein–Uhlenbeck stochastic process. All wavenumbers within a shell of radius $k_F \leqslant 2$ were subjected to forcing. The forcing amplitude, σ_F, and the correlation timescale, T_F, were set at 136.9 and 0.001, respectively. This completes the specification of the forcing used in this study.

3.3. *Parameters*

This investigation is focused on understanding dynamics of *particles* suspended in turbulence. Consequently we vary the particle parameters while keeping fixed all of the fluid parameters. The fundamental parameters that characterize the particle field are density, diameter and number density. However, alternative groupings of

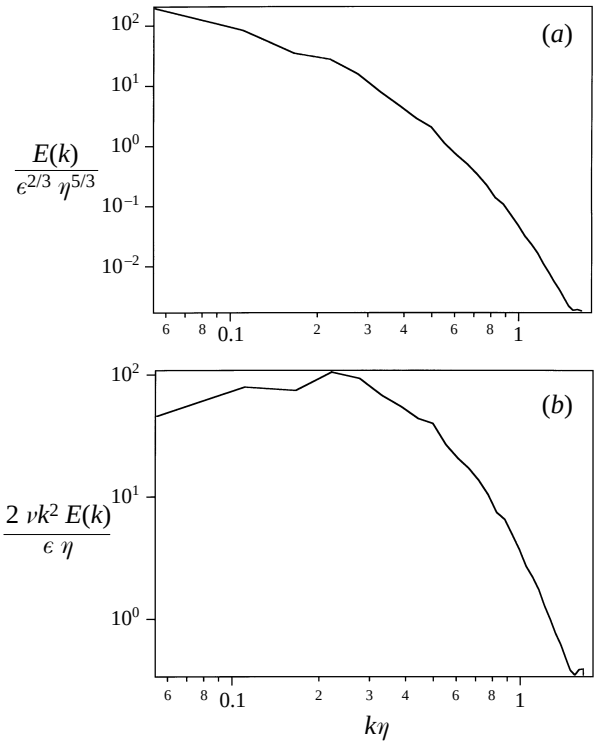

FIGURE 2. (*a*) Averaged fluid turbulent energy spectrum and (*b*) averaged viscous dissipation spectrum are plotted against a wavenumber non-dimensionalized by the Kolmogorov length scale.

these parameters can be defined to isolate the effect of specific particle properties or mechanisms. We prefer the following groupings: (i) particle response time; (ii) diameter; and (iii) number density. Appropriately non-dimensionalized forms of these parameters are the particle Stokes number $St = \tau_p/\tau_\eta$, the length scale ratio σ/η and the particle volume fraction ϕ_v.

The response time parameter, St, quantifies the particle inertia and thereby controls the degree of coupling between fluid and particulate phases. As mentioned before, at $St = 0$ the particles behave like fluid tracers with instantaneous response while at $St = \infty$ the particles are completely unresponsive to the flow. The span of the Stokes number range $(0.4, 8.0)$ is chosen such that both limiting behaviours are sampled. Extension of the simulation beyond this range poses numerical and theoretical difficulties yet to be resolved. At the low Stokes number end, there is evidence of repeated encounters between particles in the same neighbourhood as described by Sundaram & Collins (1996). These multiple collisions, an artifact of neglecting the disturbance velocities caused by the particles, can lead to spurious collision frequencies at low values of St. At high St, on the other hand, the relative velocity between the fluid and the particles increases causing the particle-based Reynolds number Re_p to significantly exceed unity. Under this condition, other terms in the particle force balance become important (e.g. Basset, pressure gradient) and therefore the particle equation of motion (3.1) must be suitably modified to include these forces.

The range of the other two particle field properties, namely the size and number of particles, are arrived at based on the simpler constraints required by our assumption

Study phenomenon	Run	St	ϕ_v	σ/η
Response time	A	1.0	4.19×10^{-3}	0.36
	B	0.4	4.19×10^{-3}	0.36
	C	2.0	4.19×10^{-3}	0.36
	D	4.0	4.19×10^{-3}	0.36
	E	8.0	4.19×10^{-3}	0.36
Number density	A	1.0	4.19×10^{-3}	0.36
	F	1.0	1.77×10^{-3}	0.36
	G	1.0	5.24×10^{-4}	0.36
Particle size	A	1.0	4.19×10^{-3}	0.36
	H	1.0	4.19×10^{-3}	0.27
	I	1.0	419×10^{-3}	0.18

TABLE 2. Particle parameters for the various runs used in this study.

of Stokes drag for the particulate phase. Particle diameters are set smaller than the Kolmogorov microscale, i.e. $\sigma/\eta < 1$. Meanwhile it is ensured that the particle densities, determined by the response time, are maintained a couple of orders of magnitude higher than the fluid density, in order that Stokes drag remains the dominant term in determining the particle trajectory. Additionally, low particle volume concentrations ($\phi_v = \frac{1}{6}\pi\sigma^3 N_p/V \ll 1$) are necessary in order to neglect modulation of the fluid phase by particles (particularly in view of the high density ratio).

3.4. *Overview of simulations*

A particle-free fluid code, under the same forcing conditions, was run for several eddy turnover times to produce a representative initial fluid velocity field. The particles were initialized at the grid points with fluid velocities. The combined system was then time advanced for over six eddy turnover times with collision statistics being averaged over the last three eddy turnover times after the particle–fluid system had equilibrated.

3.4.1. *Run organization*

The complete run chart is provided in table 2. The organization is as follows: Run A is the base run used in all three parametric studies. The set of runs (A–E) constitutes an investigation of the effect of particle response time on collision frequencies while holding particle diameter and number density constant. The particle number density was varied holding the diameter and response time constant in runs A, F, G. The effect of particle size (holding response time and number density constant) was isolated in runs A, H, I.

3.4.2. *Initialization and transition to steady state*

The forced simulations described above are intended to eliminate any influence of the initial configuration of the system on the collision statistics presented. Nevertheless, the method of initialization is important because it determines the time required for the system to 'forget' its initial state. In the present simulations, the particles were initialized at the fluid grid points and with velocities equal to the fluid velocities at those grid points. The evolution of the particle–fluid system towards a statistically stationary state was then monitored by tracking the particle-phase mean

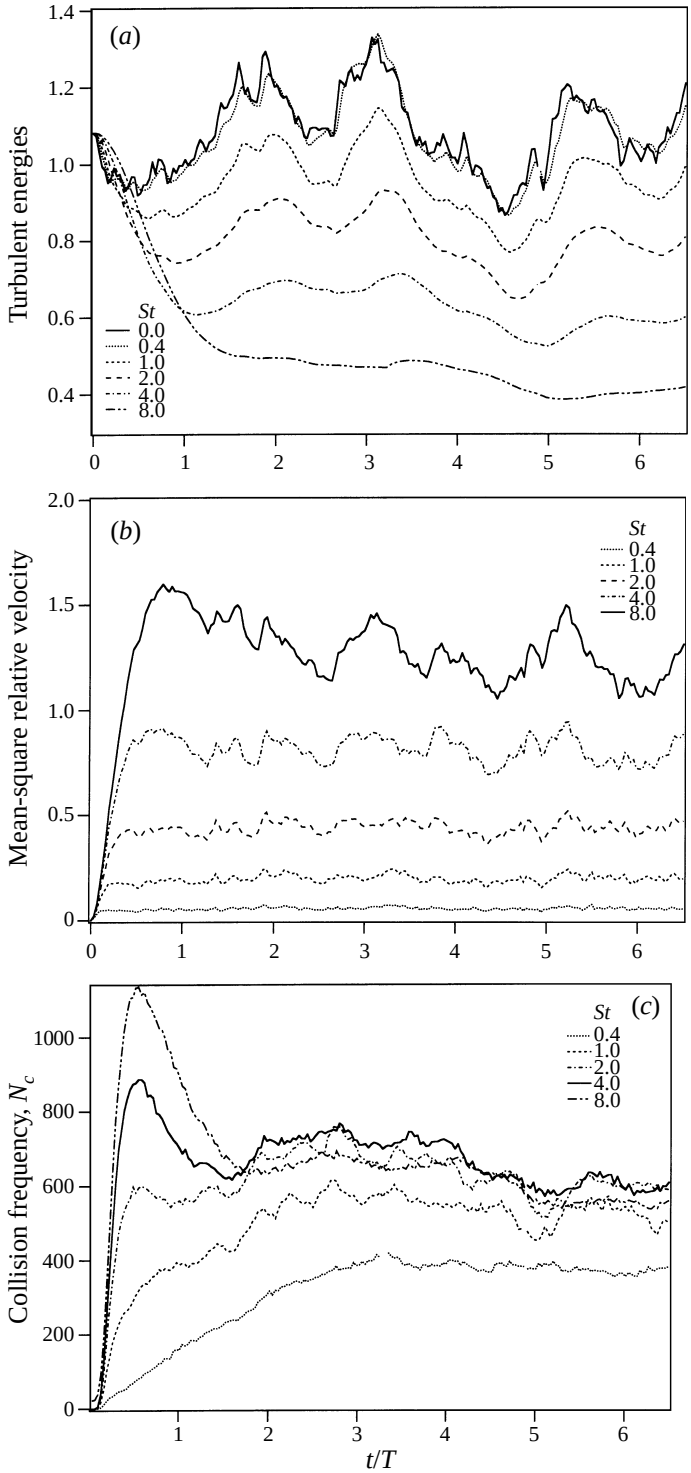

FIGURE 3. Evolution of (*a*) turbulent particle energies (*b*) mean-square slip velocity and (*c*) collision rate with time for various Stokes numbers after identical initializations. The particles reach a steady state over a time scale proportional to their response time.

St	DNS $\pm$ error	$\Phi(\tau)$ method	Extrapolated
0.4	372.28 $\pm$ 31.54	406.07	413.04
1.0	516.01 $\pm$ 33.23	518.28	526.44
2.0	584.49 $\pm$ 43.69	591.25	600.63
4.0	597.61 $\pm$ 53.28	594.65	590.45
8.0	553.52 $\pm$ 47.60	548.32	560.96

TABLE 3. Table of averaged collision frequencies as a function of Stokes number. Also shown are the collision rates calculated using (2.2) with extrapolated values and those obtained from (5.1).

kinetic energy and mean square slip velocity as a function of time. Figure 3(*a*) shows the evolution of the kinetic energy of the various particles while figure 3(*b*) plots the evolution of mean-square slip velocity over the same period of time. It can be seen that lighter particles equilibrate faster than the heavier ones, most likely because of their more rapid response times and because their initial state is closer to their equilibrium state. As the energy of the particle approaches its stationary value so does the collision frequency of the particles. Temporal fluctuations of collision frequency, for various St, are shown in figure 3(*c*). Contrary to particle energies, collision rates at lower St are observed to take longer to reach equilibrium. Nevertheless, it can be seen that all simulations reach equilibrium within a couple of eddy turnover times and therefore all statistical averages are determined after this transient period.

4. Results of direct numerical simulations

The variation of collision rates with particle Stokes number (§4.1), particle diameter (§4.2) and number density (§4.3) will be discussed in succession. Note that the effect of Stokes number is, by far, the most complex and consequently, much of the discussion to follow will be devoted to understanding this aspect.

4.1. *Effect of stokes number*

Results from the set of five runs (A–E) performed to explore the dependency of the collision frequencies on Stokes number will be presented below. Steady-state collision frequencies for these runs (described in §3.4.1) are summarized in table 3. The particle behaviour is then analysed in the context of the two theoretical limits obtained earlier: the large/dense particle ($St \to \infty$) or kinetic theory limit and the small/light particle ($St \to 0$) or Saffman–Turner limit.

Figure 4 shows the variation of the collision frequency with Stokes number as determined from the simulation. To facilitate a comparison, we have also plotted the expected values of the collision frequencies at both limits as set out in (2.4) and (2.7). Recall that the Saffman–Turner formula predicts a constant collision frequency which is a function of fluid parameters only. The kinetic theory expression is a function of both the particle kinetic energy and size; hence, this limit takes into consideration the change in the particle kinetic energy with Stokes number. The dependence of the averaged particle fluctuating energy on St is shown in figure 5. As particle inertia increases, particles are unable to follow the fluid motion entirely and therefore the intensity of particulate turbulent motion decreases with increasing particle inertia.

Firstly, it must be noted that actual collision frequencies deviate appreciably from either of the two limits over the Stokes number range considered. The Saffman–Turner

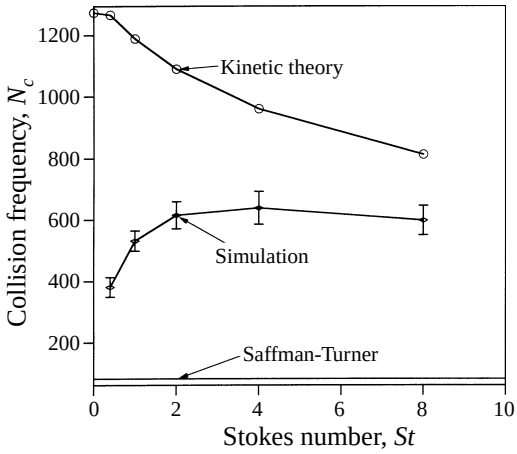

FIGURE 4. Average collision frequency as a function of Stokes number. The limiting results from the Saffman–Turner analysis ($St \to 0$, see (2.4)) and kinetic theory ($St \to \infty$, see (2.7)) are provided for the sake of comparison.

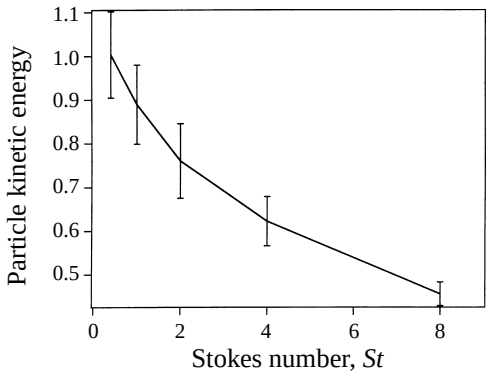

FIGURE 5. Averaged fluctuating particle energies for various Stokes numbers. Heavier particles, following less of the fluid motion, contain less turbulent energy than lighter ones.

limit, where relative motion is controlled by local velocity gradients, underpredicts the collision frequency of finite-inertia particles while the kinetic theory limit, where particle motion is completely uncorrelated, overpredicts it. Presumably, the simulations if extended would approach each of these asymptotes in the two limits. Secondly, the collision frequency is observed to reach a maximum at approximately $St = 4$ and decrease thereafter. At $St = 4$, the particle response time is approximately half the eddy turnover time and the particles are driven predominantly by the large eddies. One explanation for the maximum in collision rate is that while increasing the response time decorrelates particles from the fluid thereby enhancing the collision frequency by the more efficient 'random' collision mechanism, eventually particles become decorrelated to such an extent that they are unable to pick up energy from the fluid. The collision frequency of these 'cooler' particles is reduced by any further increase in the particle response time. The maximum appears to scale with the large-eddy turnover time.

As mentioned previously, the dynamics of finite-Stokes-number particles differ from the limits $St \to 0$ and $St \to \infty$ in two fundamental ways: (i) particles accumulate in regions of low vorticity; and (ii) relative motion between neighbouring particles

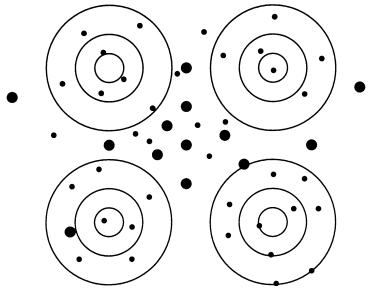

FIGURE 6. Schematic of turbulence idealized as four roll cells. Particle inertia causes heavier particles to be flung out of the circular flow regions and accumulate in the strain region in the centre. Extremely light particles will follow fluid streamlines while extremely heavy particles will be unresponsive to any flow structure and hence neither of the two will show any resultant spatial bias. This inertial mechanism causes moderately heavy particles to preferentially concentrate in strain regions and be depleted from high-vorticity regions.

is enhanced by the decorrelation of the particle motion from the fluid. Evidence for both of these effects will now be presented.

4.1.1. *Preferential concentration*

Contrary to the intuitive assumption of well-mixedness, particles distribute themselves non-uniformly in a turbulent flow field. Maxey (1987) first showed from an asymptotic analysis that, due to a mechanism of inertial bias, particles are likely to accumulate in regions of high strain and correspondingly be depleted from high-vorticity regions. In physical terms, this can be understood as due to particles, on account of their finite inertia, being flung out of vortices and collecting in strain regions as shown schematically in figure 6. Squires & Eaton (1991) followed by Wang & Maxey (1993) observed this preferential concentration of particles in certain regions of the flow in their numerical investigations of particulate turbulence. Fessler, Kulick & Eaton (1994) succeeded in observing particle aggregation in an experimental channel flow study, dispelling any doubts that this was a numerically induced phenomenon. It should be noted, however, that neither of the earlier numerical studies included inter-particle collisions.

Figure 7(*a*) shows fluid vorticity magnitude contours over a typical two-dimensional plane from our simulations. Regions with closely packed lines indicate high vorticity. Particle concentration contours for $St = 1$ over the same plane are shown in figure 7(*b*). Consistent with the inertial accumulation hypothesis, particles are seen to collect outside regions of high vorticity. Correspondingly, high-vorticity regions are consistently depleted of particles. Figure 7(*c*) plots particle concentration contours for simulated fluid tracers, $St = 0$, again over identical fluid conditions. In contrast with $St = 1$ particles, these tracer particles show no inertial bias and the figure confirms their random spatial distribution. Figure 8 shows the computed particle concentration distribution conditioned on the vorticity magnitude (normalized by its average). It is evident that at $St = 0.4$ and 1 particles are depleted in regions of high vorticity and correspondingly are concentrated in regions of low vorticity. Fluid tracers ($St = 0$), in contrast, show no correlation with the vorticity field. At high Stokes numbers ($St = 8$), once again, particles are relatively unresponsive to the intense small-scale structures and we observe little correlation with vorticity.

We now seek to quantify the non-homogeneous behaviour of particle locations. Following previous investigators, we define the particle concentration field within a

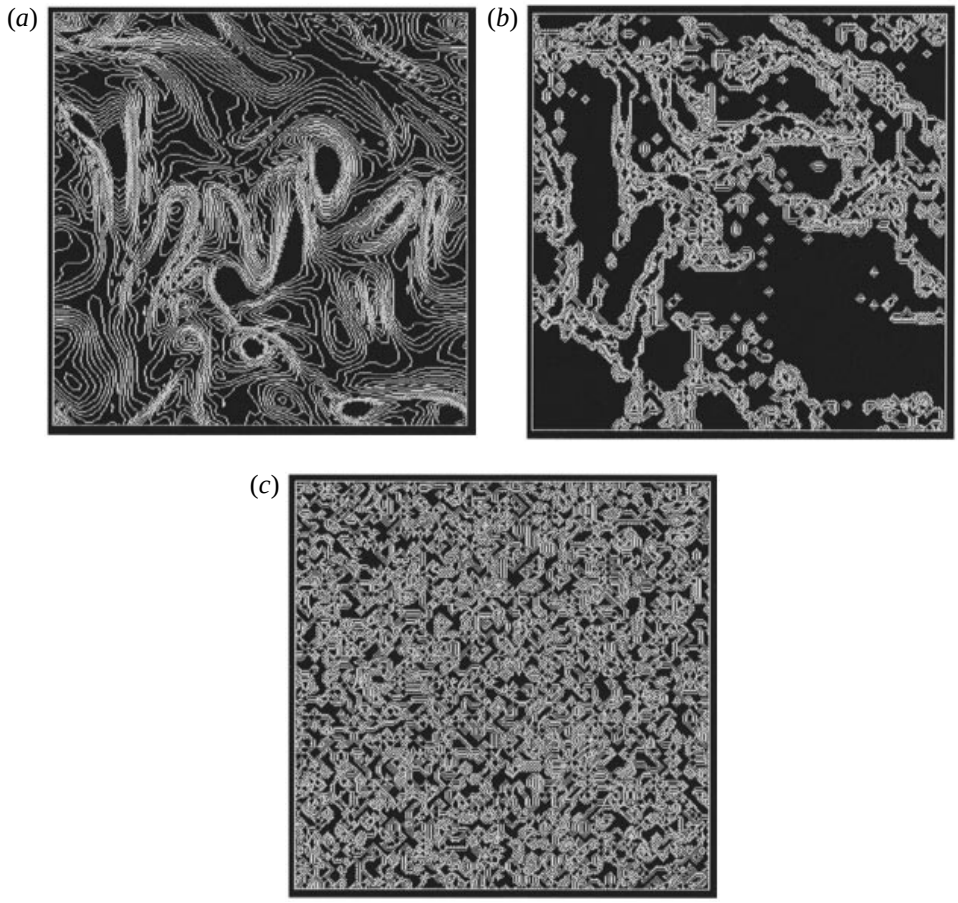

FIGURE 7. (*a*) Fluid vorticity contours over a representative two-dimensional plane (close-packed lines signify regions of high vorticity). (*b*) $St = 1$ particle concentration contours over the same plane at the same time. Notice the alignment between particle-depleted and high-vorticity regions and vice versa. (*c*) Particle concentration contours for fluid tracers ($St = 0$) indicating uniform concentration over the same plane.

sub-volume V_s as C, the number of particles found in that volume. The expected value of this concentration field, $\langle C \rangle$, is given by nV_s or N_p/N_s where N_s is the total number of subvolumes. Setting V_s equal to a grid volume, the mean concentration is found to be unity. The probability density function, $P(C)$, is then defined as the probability of finding a concentration C within a given subvolume V_s. It can be shown that for a randomly distributed system of non-interacting particles, the particle concentration has a Poisson distribution with a parameter $\lambda = \langle C \rangle$; thus, the expected number of particles in V_s is

$$P^r(C) = \frac{\lambda^C \mathrm{e}^{-\lambda}}{C!}, \quad C = 0, 1, \ldots. \tag{4.1}$$

While the above distribution is strictly true only for independent particle positions, the non-overlapping criterion does not significantly change the p.d.f. in the dilute particle concentration limit. Figure 9(*a*) shows the numerically observed particle concentration density functions for various Stokes numbers. The Poisson distribution is also shown

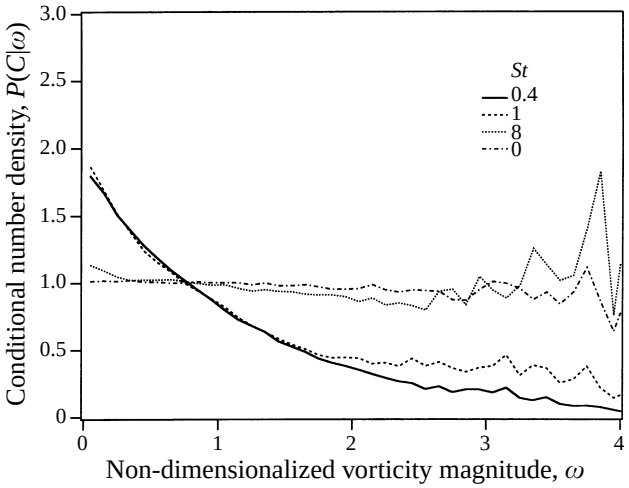

FIGURE 8. Vorticity-conditioned particle concentration p.d.f. at various Stokes numbers. Note the significant correlation between high particle concentrations and low vorticity (and vice versa) at low Stokes numbers.

for comparison. Note that all the numerical p.d.f.s deviate appreciably from the Poisson result. The simulation p.d.f.s show higher void and high concentration probabilities then the Poisson distribution, indicating a significant increase in overly accumulated and depleted regions.

A global measure of the non-uniformity of the particle concentration field is provided by comparing the numerical concentration distributions with the Poisson distribution, $P^r(C)$, signifying uniform spatial distribution of particles. For example, deviations of the concentration p.d.f. from the Poisson distribution can be measured by the sum of the square differences between the p.d.f.s:

$$D^r = \sum_C [P(C) - P^r(C)]^2, \quad C = 0, 1, \ldots$$

where $P(C)$ refers to the numerically obtained particle concentration density function. Wang & Maxey (1993) correctly argued that if preferential concentration is primarily controlled by intense vortical structures which predominate at small scales, it should obey Kolmogorov scaling. Consistent with this hypothesis, the above measure of preferential concentration is observed to reach a maximum at $St = 1$ as shown in figure 9(*b*). An identical observation was made by Wang & Maxey (1993) in their numerical study of non-interacting particles. The results of Squires & Eaton (1991), when appropriately normalized, are also consistent with the above trend.

It must be recalled that, in our formulation, the influence of non-uniform spatial distributions on the collision frequency is represented by the radial distribution function, $g(r)$. In particular, it is the RDF at contact, $g(\sigma)$, that controls the collision frequency. Figure 9(*c*) shows the RDF at contact (obtained by extrapolation as explained in §5) as a function of the particle Stokes number. Notice that the trend in the RDF profile is similar to the trend shown in figure 9(*b*), except that the maximum in the RDF occurs at $St = 0.4$, instead of at $St = 1$. The discrepancy is caused by the rapid variation of $g(r)$ near $r \approx \sigma$ (see §5). Since both the RDF (see the Appendix) and the p.d.f.s shown above quantitatively describe the non-uniform particle concentration field, the question naturally arises as to whether a relationship

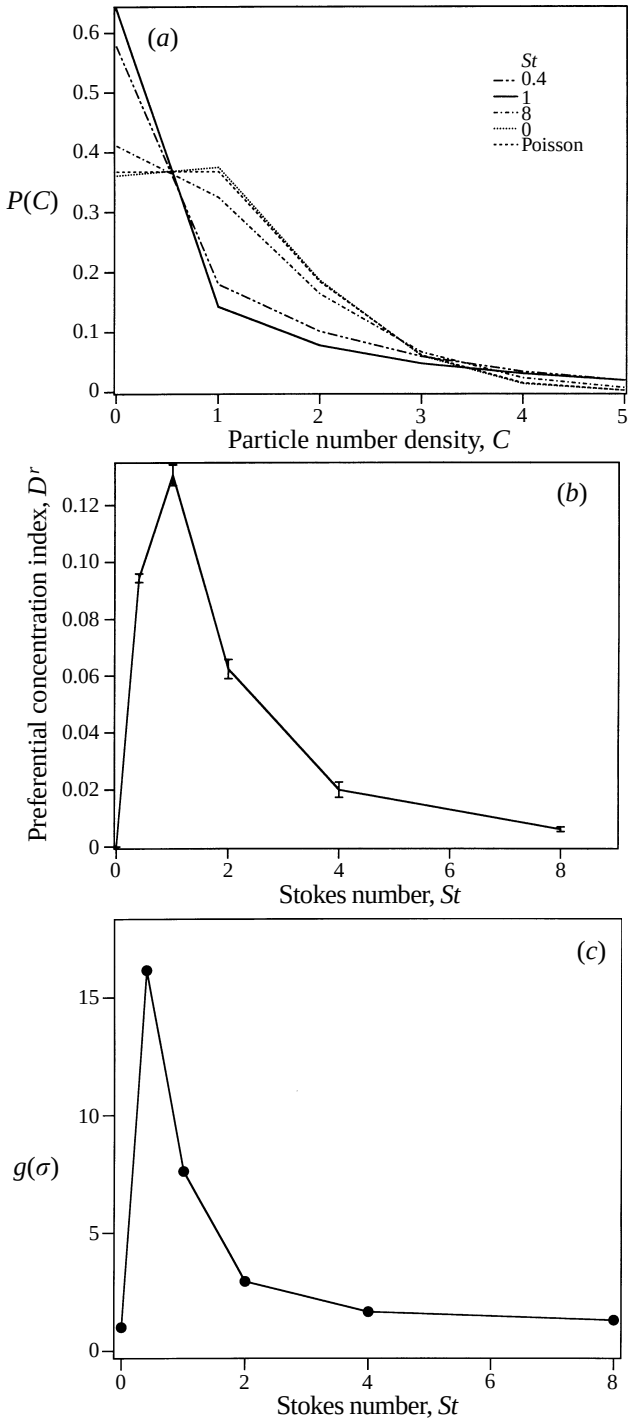

FIGURE 9. (*a*) Particle concentration density functions at a few Stokes numbers. Comparison with the Poisson distribution (for the case of randomly distributed particles) shows significant accumulation and void regions for low Stokes numbers. (*b*) Summed square deviation (D^r) of the particle concentration p.d.f.s from the Poisson distribution as a function of Stokes number. The index reaches a maximum at $St = 1$. (*c*) Particle RDF values at contact, $g(\sigma)$ as a function of Stokes number. Note that the maximum now occurs at $St = 0.4$ as opposed to $St = 1$ as in (*b*).

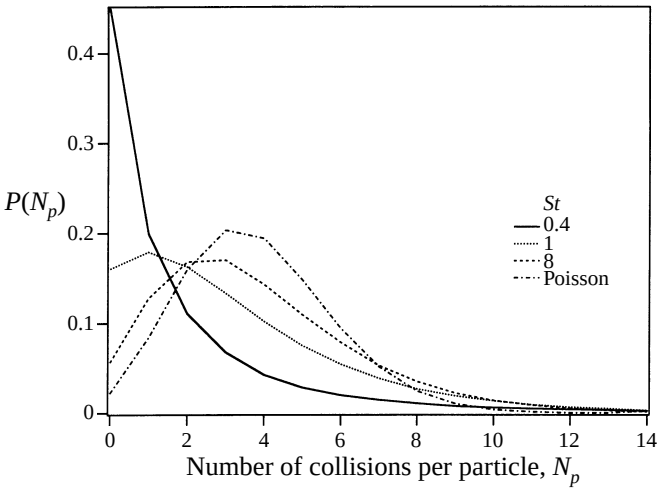

FIGURE 10. Distribution of the number of collisions per particle over the last two eddy turnover times. A Poisson distribution over the same time interval characterized by the mean collision frequency for $St = 8$ is shown for comparison.

between the two exists. That relationship can be shown to be (McQuarrie 1975)

$$\frac{\langle C^2\rangle - \langle C\rangle^2}{\langle C\rangle} = 1 + n\int_{V_s}[g(\boldsymbol{r}) - 1]\,\mathrm{d}\boldsymbol{r}$$

where again V_s is the bin volume used to compute the concentration p.d.f. and

$$\langle C^2\rangle = \int C^2\,P(C)\,\mathrm{d}C.$$

This relationship was verified (within statistical error) in our simulations.

Another indication of the effect that preferential concentration has on particle collisions is found by considering the number of collisions a given particle undergoes over the lifetime of the simulation. If the particles were randomly distributed and uncorrelated, the number of collisions experienced by a particle in a time interval $(0, t)$ also can be shown to be Poisson distributed and the fraction of particles that have undergone m collisions in the same interval is given by

$$P(m) = \frac{1}{m!}\left(\frac{t}{\tau_c}\right)^m \exp\left(-\frac{t}{\tau_c}\right)$$

where τ_c is the inverse of the averaged collision frequency. Figure 10 shows the distribution of collisions per particle computed over the last two eddy turnover times. A Poisson distribution for a collision frequency of $St = 8$ over the same interval is also plotted. It can be seen that collisions at high Stokes numbers approach a purely random process as expected for uncorrelated particles. However, at low Stokes numbers, significant fractions of particles are observed to collide repeatedly or not at all. This, presumably, is another manifestation of the phenomenon of particles, locally accumulated outside vortical structures, colliding preferentially. Thus there is further evidence to support the conclusion that, particularly near $St = 1$, strong vortical and strain flow structures disproportionately determine overall particle collision rates.

However, if particle–particle encounters are only dependent on the particle concentration field, we would expect the maximum collision frequency to occur near $St = 1$.

The fact that the maximum collision rate occurs at $St = 4$ indicates that preferential concentration is not the sole determining factor.

4.1.2. *Particle relative velocities*

Recall from the theory outlined earlier that the collision frequency in a particulate suspension is proportional to the first moment of the relative velocity distribution of *neighbouring* particles. Thus, the scale and form of these particle relative velocity distributions directly determine the collision rate.

One peculiarity of the expression for collision frequency (2.2) is that it only involves two-particle statistical properties that are conditioned on *small separation distances*. For example, the velocity distribution that is relevant for predicting particle collisions is the one conditioned on particle pairs that are in contact (nearly). One question that arises is to what degree this conditioning of the sample affects the relative velocity p.d.f. We consider this question by determining, from the simulation, a family of relative velocity p.d.f.s (normalized by the turbulence intensity) and computed over increasing radial shells, for a fixed value of the Stokes number. These are illustrated in figure 11(*a*) for a Stokes number of unity. Notice that the magnitude of the relative velocity increases with the separation distance. Furthermore, in agreement with prior experimental (Anselmet *et al.* 1984) and numerical investigations (Vincent & Meneguzzi 1993), the exponential p.d.f.s at small separations (dissipation scale) become nearly Gaussian at larger separations (integral scale).

A qualitative explanation for this behaviour can be found by considering the degree of correlation in the motion of particles separated by different distances. To illustrate this point, we consider the variance in the relative velocity of two particles separated by an arbitrary distance. Let the relative velocity vector be designated as $\boldsymbol{w} = \boldsymbol{v}_1 - \boldsymbol{v}_2$, where $\boldsymbol{v}_1$ and $\boldsymbol{v}_2$ are the velocities of each particle. The average variance of the relative velocity is then by definition

$$\overline{w^2} = \overline{v_1^2} + \overline{v_2^2} - 2\overline{\boldsymbol{v}_1 \cdot \boldsymbol{v}_2} = 2\overline{v_p^2}(1 - \chi) \tag{4.2}$$

where $\overline{v_p^2}$ is twice the mean particle kinetic energy, and the covariance coefficient χ is defined as $\chi = \overline{\boldsymbol{v}_1 \cdot \boldsymbol{v}_2}/\overline{v_p^2}$. For non-interacting particles, the Cauchy–Schwartz inequality bounds χ as

$$0 \leqslant \chi \leqslant 1$$

We expect that motion of adjacent particles will be more strongly correlated (i.e. have a larger χ) due to the influence of the fluid, while particles separated by larger distances (as compared to the Kolmogorov length scale, say) will be less correlated (i.e. have a smaller χ) because of the random nature of the turbulent fluctuations. From (4.2), this implies that relative velocities between particles that are in close proximity will be reduced by the presence of the fluid, while those between particles separated by large distances will approach the random value, $2\overline{v_p^2}$. The variance of the p.d.f.s in figure 11(*a*) increases with separation distance, in agreement with the above explanation. It must be kept in mind that the only p.d.f. that is relevant for predicting the collision frequency is the one conditioned on small separations and hence that is the one we will focus on, hereafter.

Next, the variation with Stokes number is investigated. Figure 11(*b*) graphs the relative velocity distributions of particles of varying inertia, again normalized by the fluid intensity and computed over a neighbourhood shell of radius 5σ. One apparent trend is that the width of the distribution increases as the Stokes number increases. The explanation is again related to the degree of correlation between neighbouring

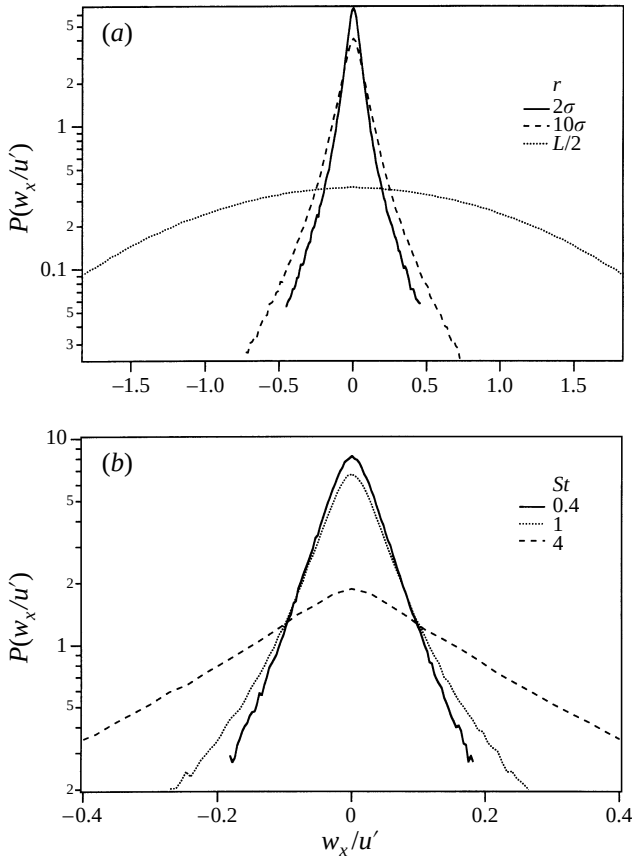

FIGURE 11. (*a*) Relative velocity (*x*-component) distribution, normalized by the fluid turbulence intensity, computed at $St = 1$ and over shells of radius 2σ, 10σ and $L/2$. Notice that the variance increases with separation distance. Furthermore, the form of the distribution approaches a Gaussian (at large separations). (*b*) Relative velocity distribution, again normalized by the fluid turbulence intensity, calculated over a radial shell of size 5σ for three different Stokes numbers. Note the increase in the variance with increasing inertia. Furthermore, the shapes of the distributions are highly non-Gaussian indicating significant correlations between the two particle velocities.

particles. At low Stokes numbers, as the particle Stokes number increases, particles become less correlated with the fluid causing the velocity of two adjacent particles to be correspondingly less correlated with each other. This leads to a decrease in the value of χ and an increase in $\overline{w^2}$. This quantity does not increase indefinitely, however, because eventually the decorrelation of the particles from the fluid will also diminish the mean particle energy, $\overline{v_p^2}$, ultimately lowering $\overline{w^2}$. Consequently, there is a maximum in the variation of $\overline{w^2}$ with Stokes number. Empirically, we observe this maximum at $\tau_p \approx T_e$ where T_e is the large-eddy turnover time, or in terms of the dimensionless parameters in the problem, $St \approx Re^{1/2}$, where Re is the *fluid* Reynolds number defined in terms of the integral length scale and the turbulence intensity.

From figure 11(*b*) we also see that the shapes of the p.d.f.s appear to belong to a family of exponential distributions, however with powers in the exponent that vary with the Stokes number. Consider the following generic, exponential p.d.f.:

$$P(w|\sigma) = \frac{n}{4\pi p^3 \Gamma(3/n)} \exp\{-(w/p)^n\}$$

where the parameter n is the exponent's power, $\Gamma(x)$ refers to the Gamma function (see Abramowitz & Stegun 1972) and p is related to the variance in the following manner:

$$p^2 = \frac{\Gamma(3/n)}{\Gamma(5/n)} \overline{w^2}.$$

At very small values of the Stokes number, the p.d.f. has a nearly perfect exponential shape, corresponding to $n = 1$, while at large Stokes numbers the p.d.f. approaches a Gaussian form corresponding to $n = 2$. Unfortunately, the progression of the exponent between the two limits is not monotonic. Instead, we observe that at small but finite Stokes numbers, the exponent decreases with increasing Stokes number, reaching a minimum near $St = 1$, and then increases thereafter, approaching the value 2 at the largest Stokes numbers in the study. Expectedly, at low St, particle p.d.f.s are similar to the exponential ones observed for fluid relative velocities at small separations, as previously seen in figure 11(a). The motion of heavy particles, on the other hand, is dominated by their interactions with the large eddies. It can be argued that, as a consequence of the central limit theorem, their relative velocities should be Gaussian distributed. However, the behaviour of the p.d.f.s at moderate Stokes numbers is complex and difficult to explain. It is most likely connected to the strongly inhomogeneous particle concentration field associated with systems near $St = 1$. Unfortunately, there is little theoretical foundation for analysing systems that are very far from statistical equilibrium, thus we only suggest these qualitative arguments as a possible explanation.

4.1.3. *Summary*

The picture that emerges is as follows: at low Stokes numbers, the collision frequency increases with St due to both an increase in the relative velocity of neighbouring particles and preferential concentration of particles in low-vorticity regions of the flow. However, the effect due to preferential concentration reaches a maximum at $St = 0.4$, and decreases thereafter. Thus, the continued rise in the collision frequency for $St > 0.4$ is attributed entirely to the increase in the relative velocities between particles. Eventually the collision frequency will peak at a Stokes number that scales like $Re^{1/2}$ (or when $\tau_p \approx T_e$) and decrease thereafter as the loss in particle energy offsets the increase due to the decorrelation of the particle velocities. We therefore conclude that although the collision frequency for particles with small Stokes numbers is determined entirely by the Kolmogorov-scale parameters, the location and magnitude of the maximum particle collision frequency is more strongly correlated with the turbulent motions at the integral scale.

The collision frequency in a particle suspension involves a complex interplay of the particle concentration field and the mechanisms responsible for relative motion between the particles. Theoretical treatments must capture both phenomena. Part 2 of this paper (Sundaram & Collins 1997) will present a theoretical approach to predicting the collision frequency based on predictions of $g(\sigma)$ and $P(w|\sigma)$.

4.2. *Effect of diameter*

Bearing in mind that the formulation of the particle equation of motion restricts us to considering $\sigma/\eta < 1$, we compared collision frequencies at three different particle diameters. The particle Stokes number was maintained at unity for the same reasons as explained in the previous subsection. As discussed in §2 and the Appendix, particles of diameter σ present an effective collision cross-section proportional to σ^2. However

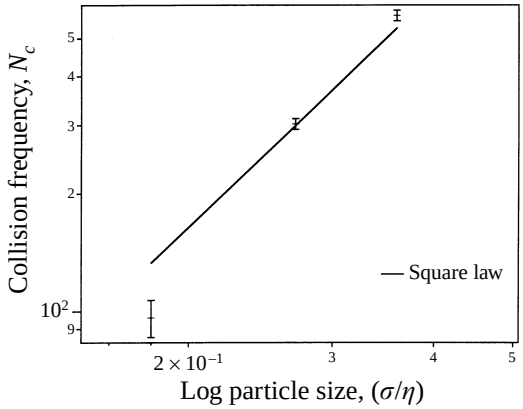

FIGURE 12. Effect of particle size on collision frequency. The observed collision frequency, while following a squared dependence on particle diameter at larger sizes, indicates a steeper falloff ($\propto \sigma^3$) at smaller sizes, consistent with Saffman's limiting result (2.4).

the mechanism for collision in the Saffman–Turner limit (small size) requires a velocity gradient to cause relative motion between the particles resulting in a cubic dependence on the particle diameter (see (2.4)). At larger values of the particle diameter, relative velocities are controlled by a random kinetic-like mechanism. Consistent with the above thinking, figure 12 shows that the collision frequency is observed to follow a square dependence at sizes approaching the Kolmogorov scale while deviating to a higher ($\sim \sigma^3$) dependence at a smaller size.

4.3. *Effect of number density*

A comparison of collision frequencies at various particle number densities was done at $St = 1$ and $\sigma/\eta = 0.36$ (Runs A, F and G). Maintaining the same particle response time ensures that the dynamic spatial and velocity distributions of particles remain identical. If the particles are completely independent of each other, i.e. no hydrodynamic or other interactions, the overall particle number density serves merely as a scaling factor (see 2.2). Figure 13 shows a logarithmic plot of the collision frequencies vs. the log of the number density. The solid line is the square-law and the simulations confirm the square law behaviour of collision frequencies with particle number density. It must be noted that this result may change at very high number densities when the particle volume fraction is appreciable. At higher concentrations, particles will screen each other causing a deviation from the square law.

5. Confirmation of equation (2.2)

Collision frequencies between particles depend on the static particle parameters such as size, density and average concentration and also on dynamic properties such as spatial and velocity distributions which are controlled by interactions with the fluid. However, based on the results presented in § 4, it appears that the critical question is the dependence on the particle inertia or equivalently the particle Stokes number. Recall that the collision frequency can be rigorously defined in terms of two statistical properties of the particle field, $g(\sigma)$ and $P(w|\sigma)$ (see (2.2)). In this section, we check the validity of (2.2), by substituting $g(\sigma)$ and $P(w|\sigma)$ determined from the DNS.

In this case, we would expect nearly exact agreement between the values found directly from the simulations and the ones computed from (2.2). Unfortunately, one

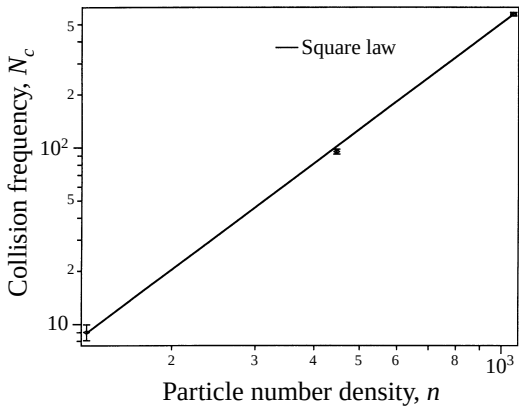

FIGURE 13. Collision frequencies are observed to follow the conventional squared dependence as a function of the particle number density.

difficulty with using (2.2) in its present form is that it requires statistics on fluid volumes immediately adjacent to the particles. Because particle pairs rarely lie in these small volumes, the statistical noise (relative to the signal) becomes significant and the reliability of $g(\sigma)$ becomes questionable. Furthermore at the lowest values of the Stokes number, the rapid variation of $g(r)$ around $r = \sigma$ makes it difficult to extrapolate the value of $g(\sigma)$ from the nearest points. Note, one cannot evaluate $g(\sigma)$ directly, but rather $g(\sigma + \epsilon)$, where $\epsilon > 0$. Extrapolating to the value at $r = \sigma$ is necessary, particularly for the lowest Stokes number cases where $g(r)$ varies rapidly. This is illustrated in figure 14 which shows a plot of $g(r)$ at several Stokes numbers. Notice that the curves at the two lowest Stokes numbers vary rapidly near $r = \sigma$. Thus, there is some uncertainty in estimating $g(\sigma)$ from the simulation database.

A preferred approach uses an integral formulation for the number of collisions that occur over a finite time τ (see the Appendix for a derivation):

$$Z_c(\tau) = \pi n^2 \int \int_0^\infty \Phi(\tau; r, w) g(r) P(w|r) r^2 \, \mathrm{d}r \, \mathrm{d}\boldsymbol{w} \tag{5.1}$$

where $Z_c(\tau)$ is the total number of collisions over the entire particle system in the time interval $(0, \tau)$ and

$$\Phi(\tau; r, w) = \begin{cases} 0, & w \leqslant \dfrac{r - \sigma}{\tau} \\ 1 + \dfrac{\sigma^2 - r^2 - w^2\tau^2}{2rw\tau}, & \dfrac{r - \sigma}{\tau} \leqslant w \leqslant \dfrac{(r^2 - \sigma^2)^{1/2}}{\tau} \\ 1 - \left(1 - \dfrac{\sigma^2}{r^2}\right)^{1/2}, & w \geqslant \dfrac{(r^2 - \sigma^2)^{1/2}}{\tau}. \end{cases}$$

The slope of $Z_c(\tau)$ at $\tau = 0$ is by definition the collision frequency, N_c. The advantage of using (5.1) rather than (2.2) is that the collision frequency is determined by an *integral* of the RDF.

Evaluating (5.1) still requires a functional relationship for the RDF over the radial domain $\sigma \leqslant r \leqslant \infty$. In particular, the integral was found to be sensitive to the RDF in the neighbourhood of $r = \sigma$ (where no data exist). In view of the difficulty of obtaining particle statistics at small separations and the rapid variation of the RDF at distances close to σ (at small Stokes numbers), we decided to use a locally

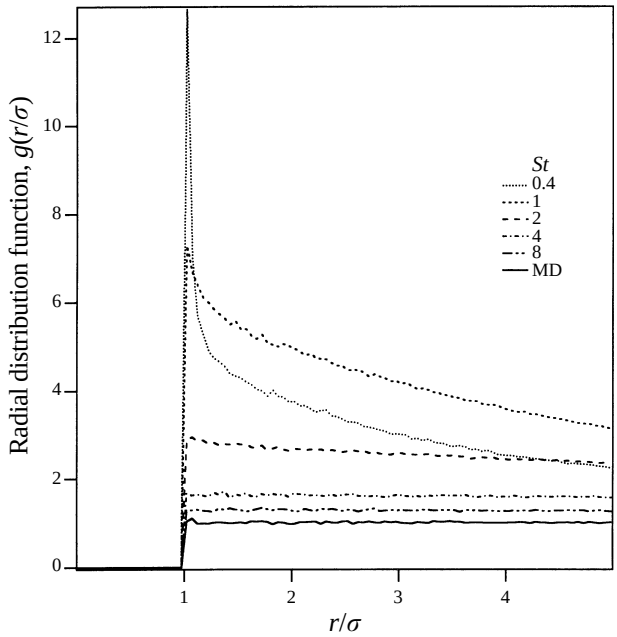

FIGURE 14. Radial distribution functions (RDF) upto 5σ for various Stokes numbers. The RDF for a randomly distributed particle system is plotted for comparison.

extrapolated form for $g(r)$ for distances smaller than the first numerically evaluated point. The numerical values were then used at larger radial distances. For distances smaller than the first datum point, the RDF was expanded in the following power series:

$$g(r) = \sum_{n=0}^{M} a_n \left(1 - \frac{\sigma}{r}\right)^n. \tag{5.2}$$

The value of M, which depends on the number of numerical points used in the fit, was typically taken to be unity, although the results were found to not vary significantly if M was set to 2 or 3. $P(w|r)$ was not extrapolated for very short distances owing to noise in the data. However, as $P(w|r)$ shows a weaker dependence on r than $g(r)$, this is not expected to cause significant error in the calculation.

Figure 15(a) shows the variation of $Z_c(\tau)$ with τ for different Stokes numbers. Figure 15(b) is an enlargement at very small τ. There is an extended straight line region at small τ as a result of RDF extrapolation. Also, the curves become noisier at larger values of τ owing to the noise in the numerical curves for $g(r)$ and $P(w|r)$. The collision frequency, given by the slope at $\tau = 0$, was determined from the graph and is illustrated in figure 16 along with the observed collision frequency from the simulations. As expected, there is good agreement between the two curves. Moreover, a comparison of the collision frequency computed from (5.1) with one computed from (2.2), using extrapolated values for both $g(\sigma)$ (from (5.2), $g(\sigma) = a_0$) and $\overline{w}|_\sigma$ are nearly identical. The agreement of the two approaches gives us additional confidence in the extrapolation technique. Moreover, the agreement in figure 16 suggests that the best strategy for predicting the collision frequency is to predict $g(\sigma)$ and $P(w|\sigma)$.

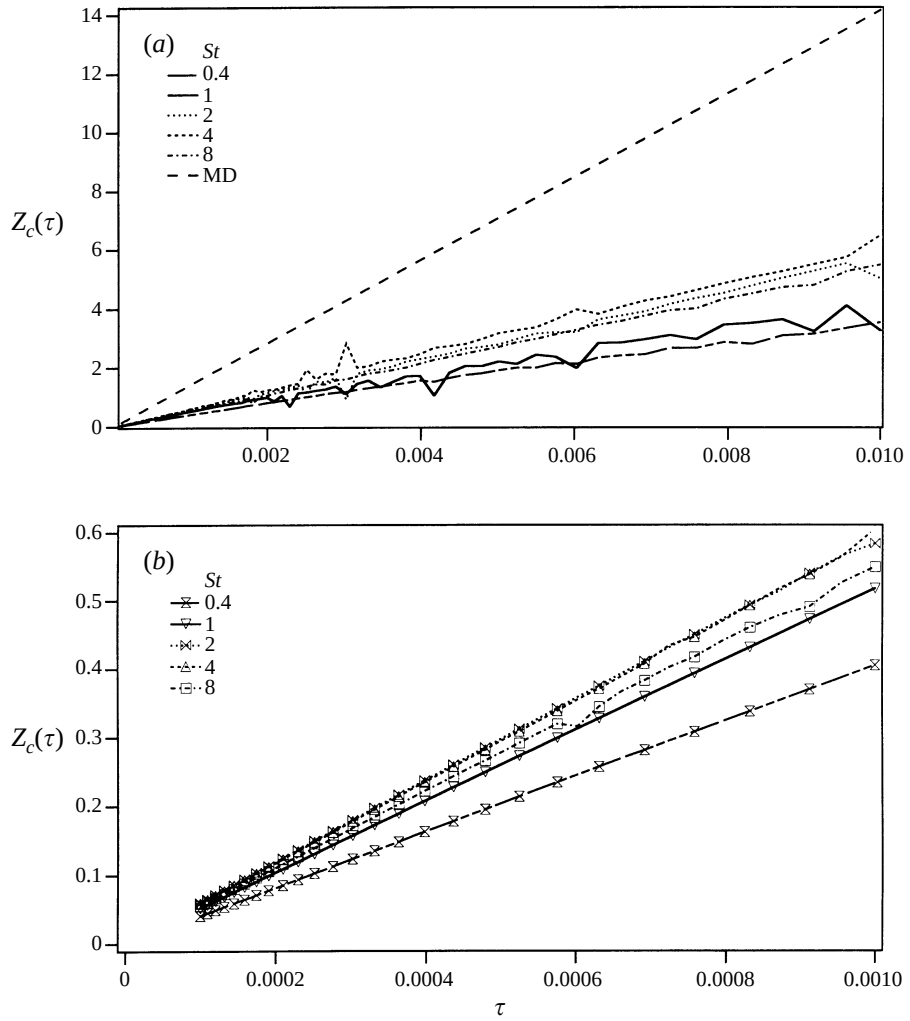

FIGURE 15. (*a*) Variation of $Z_c(\tau)$ with τ for various Stokes numbers. Noise at large τ is due to fluctuations in the particle data. The slope of this function at small τ yields the collision frequency. (*b*) An enlargement of the small-τ region. The remarkably linear behaviour is directly attributable to the smooth extrapolated data.

6. Summary

Direct numerical simulations of a finite-volume particle suspension, including elastic collisions between particles, were performed on a 64^3 lattice for the fluid and with 64^3 particles. The influence of particle parameters such as response time, particle diameter, and number density on collision frequency in a monodisperse particle system was investigated. The observations were then interpreted in terms of two limiting theories: (i) the Saffman–Turner analysis valid for $St \to 0$ and (ii) the kinetic theory valid for $St \to \infty$. It was discovered that although both theories apparently work in their appropriate limits, the collision frequency for particles at intermediate values of Stokes number differed significantly from either. In particular, it was found that the collision rate increased sharply with Stokes number at small values, peaked at a value corresponding to $\tau_p \approx T_e$ and then de-

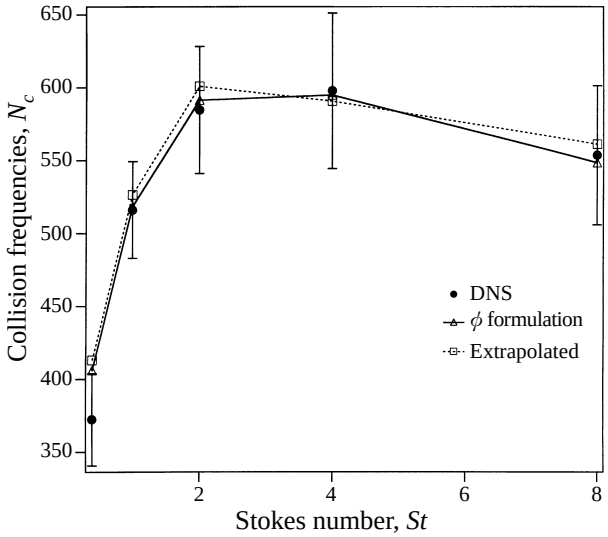

FIGURE 16. Comparison of DNS collision frequencies with values calculated from (2.2) in conjunction with particle data from the simulations and values calculated using the slope of $Z_c(\tau)$ at small τ. Notice the good agreement amongst all three values.

creased, approaching the kinetic theory expression at large Stokes numbers. The complex behaviour with Stokes number is ultimately traced to two effects: (i) particles with finite inertia collect in regions of low vorticity leading to a highly non-uniform particle concentration field and (ii) particle inertia affects the degree of correlation in the velocity of two adjacent particles thereby altering their relative velocity.

Each effect can be related to a single statistical property in the formula for the collision frequency (2.2). First, the non-uniform concentration field of the particles alters the RDF at contact, $g(\sigma)$. Second, the decorrelation of adjacent particle motions affects the relative velocity p.d.f., $P(w|\sigma)$. The final observed collision frequency can therefore be thought of as a complex interplay between both effects. At low Stokes numbers, the collision frequency increases with Stokes number because it enhances the RDF *and* the particle relative velocities. However, as the Stokes number continues to increase, first preferential concentration will begin to decline because the particles become too heavy to be strongly affected by the local vorticity (this occurs at $\tau_p \approx \tau_\eta$), and then eventually the relative velocities decrease because particles become ineffective at picking up energy from the fluid, thus their motion (relative motion and otherwise) will decline (this occurs at $\tau_p \approx T_e$). The latter effect is dominant at high Stokes numbers.

The dependence of collision frequency on the particle diameter (holding Stokes number and number density fixed) was also determined. A naive examination of (2.2) might suggest a square dependence on the diameter, however a logarithmic plot shows a more complex behaviour. That complexity arises from the effect that diameter has on $g(\sigma)$ and $P(w|\sigma)$. The effect on the former is relatively obvious (since the value of σ is an argument), while the latter is due to a change in the mechanism responsible for producing relative motion between neighbouring particles. Gradient-driven collisions (Saffman–Turner mechanism) dominate for small particles and scale with the cube of

the diameter while the random kinetic mechanism is more effective for larger particles leading to a square dependence on diameter. The result is that the collision frequency increases as the cube of the diameter at small diameters but changes to a square dependence at large diameters.

Finally, the effect of the number density (holding the Stokes number and diameter fixed) was determine from the simulations. The collision frequency was found to obey a 'square law' for all simulations considered in this study. Thus, we conclude that as long as the volume fraction of particles is low (10^{-4} in this case) the 'dilute' assumptions are valid and therefore there is no direct effect of number density on the collisional parameters $g(\sigma)$ and $P(\boldsymbol{w}|\sigma)$.

The exact expression for collision frequency derived in this study, (2.2), was verified by calculating the necessary statistical properties from the DNS database. There was some difficulty in evaluating statistics precisely at $r = \sigma$ and extrapolation was required. This was particularly troublesome for Stokes numbers near unity where rapid variation of the RDF with r/σ near 1 was observed. An alternative expression for the number of collisions over a finite time period was developed, (5.1), that involved integrals over the entire spatial domain. The advantage of this formulation is that it does not rely on statistics evaluated at $r/\sigma = 1$. The collision frequency is then by definition given by the slope of this function at $\tau = 0$. A comparison of the collision frequency obtained by extrapolation using (2.2) and from the slope of collision function agreed with each other and with the values from the numerical simulations, confirming both relationships. The agreement between the values obtained from (2.2) with those obtained from (5.1) also confirms the extrapolation technique used in this study.

The ultimate goal of this study is to develop a methodology for predicting the collision frequency based on knowledge of the relevant turbulence parameters and the particle physical properties. Equation (2.2) and the results presented in §5 suggest that predicting the collision frequency is equivalent to predicting the two statistical properties of the particle phase, $g(\sigma)$ and $P(w|\sigma)$. A strategy for estimating these two statistics is the subject of Part 2 of this article (Sundaram & Collins 1997). It is interesting to note that the collision frequency is completely described by the statistical properties of particle pairs conditioned on being (nearly) in contact. This implies that corrections to the theory to account for short-range repulsive forces between the particles (Sundararajakumar & Koch 1996) can be incorporated into (2.2). These forces will appear as an energy barrier (activation energy) that the particles' relative velocity must overcome. Particle pairs with relative velocities (along the centres) below the given threshold simply will not contact each other. The theory can account for this activation energy by limiting the integration in (2.2) to values of $|\boldsymbol{w}|$ that exceed the threshold.

The authors gratefully acknowledge financial support for this study from Dow Chemical, through the Young Minority Investigator Award (awarded to L.R.C.).

Appendix. Collision frequency formulation

The collision frequency can be expressed exactly in terms of two statistical properties of the particle phase, $g(\sigma)$ and $P(\boldsymbol{w}|\sigma)$. The purpose of this appendix is to derive that relationship. We begin by developing an expression for a collision operator whose sole purpose is to determine whether two particles will collide in a time τ (yielding the value of unity if they will collide and zero if not), given the initial particle positions

and velocities, under the assumption that the velocities do not change in time. Mean collision frequencies can then be determined by performing an appropriate statistical average of the collision operator over all possible particle locations and velocities. Each aspect is considered below separately.

A.1. *Collision operator*

Consider two particles located at positions $\boldsymbol{x}_1$ and $\boldsymbol{x}_2$ and moving with velocities $\boldsymbol{v}_1$ and $\boldsymbol{v}_2$. We can define a relative coordinate and velocity as shown below

$$\boldsymbol{r} = \boldsymbol{x}_1 - \boldsymbol{x}_2, \quad \boldsymbol{w} = \boldsymbol{v}_1 - \boldsymbol{v}_2$$

If we assume the particles are in 'free flight', that is, their velocities remain constant, the separation vector will obey the following relationship:

$$\boldsymbol{r}(t) = \boldsymbol{r}(0) + \boldsymbol{w}t$$

or equivalently, the separation distance is given by

$$r(t) = (r^2(0) + 2(\boldsymbol{r}(0) \cdot \boldsymbol{w})t + w^2t^2)^{1/2} \tag{A 1}$$

The time required to reach the minimum separation distance between the particles, t^* (corresponding to when $\mathrm{d}r(t)/\mathrm{d}t = 0$) is given by

$$t^* = -\frac{(\boldsymbol{r} \cdot \boldsymbol{w})|_0}{w^2}. \tag{A 2}$$

Determining whether two particles will collide over the time interval $0 \leqslant t \leqslant \tau$ can be interpreted as determining whether the separation distance over that interval is ever less than the particle diameter σ , i.e. is $r(t) \leqslant \sigma$ for $0 \leqslant t \leqslant \tau$. Consequently, we should test for collisions when the particles have reached their minimum separation distance. Equation (A2) expresses the time required to reach the minimum separation distance, however this does not consider the possibility that the time t^* may lie outside the time interval of interest $0 \leqslant t \leqslant \tau$. We therefore define the time to minimum separation within the time interval $0 \leqslant t \leqslant \tau$, t^* as follows:

$$\tau^* = H(t^*)\left[t^* + (\tau - t^*)H(t^* - \tau)\right] \tag{A 3}$$

where H is the Heaviside function. The collision operator can then be defined in the following manner:

$$\Phi(\boldsymbol{r}, \boldsymbol{w}; \tau) = H[\sigma - r(\tau^*)]. \tag{A 4}$$

A.2. *Statistical properties of the particle phase*

Consider an ensemble of systems each with N monodisperse particles in a constant volume V. The probability that particle 1 lies between $\boldsymbol{x}_1$ and $\boldsymbol{x}_1 + \mathrm{d}\boldsymbol{x}_1$, moving with a velocity between $\boldsymbol{v}_1, \boldsymbol{v}_1 + \mathrm{d}\boldsymbol{v}_1$ etc. is represented as $P^{(N)}\left(\boldsymbol{x}_{1,\ldots,N}, \boldsymbol{v}_{1,\ldots,N}\right)$. This probability is subject to the standard normalization

$$\int P^{(N)}\left(\boldsymbol{x}_{1,\ldots,N}, \boldsymbol{v}_{1,\ldots,N}\right) \; \mathrm{d}\boldsymbol{x}_{1,\ldots,N} \, \mathrm{d}\boldsymbol{v}_{1,\ldots,N} = 1.$$

Given that a collision is a two-particle event, we can define the collision frequency in terms of the two-particle probability

$$P^{(2)}(\boldsymbol{x}_1, \boldsymbol{x}_2, \boldsymbol{v}_1, \boldsymbol{v}_2) = \int P^{(N)}\left(\boldsymbol{x}_{1,\ldots,N}, \boldsymbol{v}_{1,\ldots,N}\right) \; \mathrm{d}\boldsymbol{x}_{3,\ldots,N} \, \mathrm{d}\boldsymbol{v}_{3,\ldots,N}.$$

Alternatively, we can define the two-particle probability in terms of average and relative positions

$$P^{(2)}(\boldsymbol{x},\boldsymbol{r},\boldsymbol{G},\boldsymbol{w}) = P^{(2)}\left(\boldsymbol{x}+\frac{1}{2}\boldsymbol{r},\boldsymbol{x}-\frac{1}{2}\boldsymbol{r},\boldsymbol{G}+\frac{1}{2}\boldsymbol{w},\boldsymbol{G}-\frac{1}{2}\boldsymbol{w}\right)$$

where $\boldsymbol{r}$ and $\boldsymbol{w}$ are as defined previously, and $\boldsymbol{x}$ and $\boldsymbol{G}$ are given by

$$\boldsymbol{x} = \frac{\boldsymbol{x}_1+\boldsymbol{x}_2}{2}; \quad \boldsymbol{G} = \frac{\boldsymbol{v}_1+\boldsymbol{v}_2}{2}.$$

Assuming the particles are indistinguishable, let us now define the expression for the average number of collisions per unit volume over a time period τ:

$$Z_c(\tau) = \frac{1}{2}\frac{N(N-1)}{V}\int\int\int\int \Phi(\boldsymbol{r},\boldsymbol{w};\tau)P^{(2)}(\boldsymbol{x},\boldsymbol{r},\boldsymbol{G},\boldsymbol{w})\ \mathrm{d}\boldsymbol{x}\,\mathrm{d}\boldsymbol{r}\,\mathrm{d}\boldsymbol{G}\,\mathrm{d}\boldsymbol{w}.$$

For a statistically homogeneous volume the integrations with respect to $\boldsymbol{x}$ and $\boldsymbol{G}$ can be performed directly, reducing the expression to

$$Z_c(\tau) = \frac{1}{2}\frac{N(N-1)}{V}\int\int \Phi(\boldsymbol{r},\boldsymbol{w};\tau)P^{(2)}(\boldsymbol{r},\boldsymbol{w})\ \mathrm{d}\boldsymbol{r}\,\mathrm{d}\boldsymbol{w}. \tag{A 5}$$

Note, the arguments in the p.d.f. indicate the remaining free variables, all others having been integrated out. Equation (A5) can be re-expressed in terms of a conditional probability as

$$Z_c(\tau) = \frac{1}{2}\frac{N(N-1)}{V}\int\int \Phi(\boldsymbol{r},\boldsymbol{w};\tau)P(\boldsymbol{w}|\boldsymbol{r})P^{(2)}(\boldsymbol{r})\,\mathrm{d}\boldsymbol{r}\,\mathrm{d}\boldsymbol{w}$$

where $P(\boldsymbol{w}|\boldsymbol{r})$ is the conditional probability. One can now introduce the radial distribution function in the collision relationship by noting that

$$g(\boldsymbol{r}) = \frac{N(N-1)}{n^2V}P^{(2)}(\boldsymbol{r})$$

and hence

$$Z_c(\tau) = \tfrac{1}{2}n^2\int\int \Phi(\boldsymbol{r},\boldsymbol{w};\tau)P(\boldsymbol{w}|\boldsymbol{r})g(\boldsymbol{r})\,\mathrm{d}\boldsymbol{r}\,\mathrm{d}\boldsymbol{w} \tag{A 6}$$

Equation (A6), which is an exact expression for the number of collisions in a time τ, becomes the starting point for deriving the two expressions for the instantaneous rate of collision (2.2) or the number of collisions in a finite time τ. The derivation of each expression is shown below.

A.3. *Instantaneous expression (2.2)*

The expression for the collision frequency (A6) implicitly assumes that the particles will not undergo any accelerations between collisions, which is manifestly false for particles suspended in a fluid. Thus, (A6) can only be considered valid for vanishingly small values of τ, such that particle velocities will not have changed very much. Accordingly, we must define the collision *frequency* as a limit, as $\tau \to 0$

$$N_c = \lim_{\tau\to 0}\frac{Z_c(\tau)}{\tau} = \frac{\mathrm{d}Z_c(0)}{\mathrm{d}\tau}$$

where N_c is the number of collisions per unit time and volume. Since the limits of the integrations in (A6) are not functions of τ, differentiating (A6) with respect to τ is

identical to differentiating the integrand. Differentiating the function $\Phi(\boldsymbol{r}, \boldsymbol{w}; \tau)$ yields the following

$$\frac{\mathrm{d}\Phi(\boldsymbol{r}, \boldsymbol{w}; 0)}{\mathrm{d}\tau} = -\frac{(\boldsymbol{r} \cdot \boldsymbol{w})}{r(0)} H(t^*)\delta[\sigma - r(0)]. \tag{A 7}$$

Substituting (A7) into (A6) and integrating over the $\boldsymbol{r}$ coordinate (assuming the system is isotropic) results in an expression for the collision frequency, as shown below

$$N_c = \tfrac{1}{2}\pi\sigma^2 n^2 g(\sigma) \int w\, P(\boldsymbol{w}|\sigma)\, \mathrm{d}\boldsymbol{w}.$$

A.4. *Collision rates for small but finite* τ

As noted in the text, it is sometimes desirable to determine the collision frequency over times, τ, that are perhaps small (as compared to τ_p) but finite because of the difficulty in determining statistics such as $g(\sigma)$ precisely at $r = \sigma$. The expression for the collision frequency for small but finite τ can be found by reconsidering (A6), however in this case without applying the limit $\tau \to 0$. For an isotropic system, the integration over the solid angle $\mathrm{d}\Omega_r$ can be performed analytically. The only term in the integrand that is a function of the solid angle is $\Phi(\boldsymbol{r}, \boldsymbol{w}; \tau)$, which upon integration becomes

$$\Phi(r, w; \tau) = \begin{cases} 0, & w \leqslant \dfrac{r - \sigma}{\tau} \\ 1 + \dfrac{\sigma^2 - r^2 - w^2\tau^2}{2rw\tau}, & \dfrac{r - \sigma}{\tau} \leqslant w \leqslant \dfrac{(r^2 - \sigma^2)^{1/2}}{\tau} \\ 1 - \left(1 - \dfrac{\sigma^2}{r^2}\right), & w \geqslant \dfrac{(r^2 - \sigma^2)^{1/2}}{\tau}. \end{cases} \tag{A 8}$$

The collision frequency is then obtained as

$$N_c(\tau) = \pi n^2 \int r^2 \frac{\Phi(\tau; r, w)}{\tau} g(r) P(\boldsymbol{w}|r)\, \mathrm{d}r\, \mathrm{d}\boldsymbol{w}.$$

It is possible to show that (A8) approaches (A7) in the limit as $\tau \to 0$, confirming the consistency of the two approaches. Moreover, (A8) involves a spatial integral over the entire r-domain rather than depending solely on statistics at $r = \sigma$, making it attractive for evaluating statistical properties from simulation data that contain significant statistical noise.

REFERENCES

Abrahamson, J. 1975 Collision rates of small particles in a vigorously turbulent fluid. *Chem. Engng Sci.* **30**, 1371–1379.

Abramowitz, M. & Stegun, I. A. 1972 *Handbook of Mathematical Functions.* Dover.

Allen, M. P. & Tildesley, D. J. 1987 *Computer Simulation of Liquids.* Oxford University Press.

Anselmet, F., Gagne, Y., Hopfinger, E. J. & Antonia, R. A. 1984 High-order velocity structure functions in turbulent shear flows. *J. Fluid Mech.* **140**, 63–89.

Balachandar, S. & Maxey, M. R. 1989 Methods for evaluating fluid velocities in spectral simulations of turbulence. *J. Comput. Phys.* **83**, 96–125.

Batchelor, G. K. & Green, J. T. 1972 The hydrodynamic interaction of two small freely-moving spheres in a linear flow field. *J. Fluid Mech.* **56**, 375–400.

Brooke, J. W., Hanratty, T. J. & McLaughlin, J. B. 1994 Free flight mixing and deposition of aerosols. *Phys. Fluids* **6**, 3404–3415.

Brooke, J. W., Kontomaris, K., Hanratty, T. J. & McLaughlin, J. B. 1992 Turbulent deposition and trapping of aerosols at a wall. *Phys. Fluids* A **4**, 825.

Canuto, C., Hussaini, M. Y., Quarteroni, A. & Zang, T. A. 1988 *Spectral Methods in Fluid Dynamics*. Springer.

Curtis, A. S. & Hocking, L. M. 1970 Collision efficiency of equal spherical particles in a shear flow. *Trans. Faraday Soc.* **66**, 1381–1390.

Davis, R. H. 1984 The rate of coagulation of a dilute polydisperse system of sedimenting spheres. *J. Fluid Mech.* **145**, 179–199.

Elghobashi, S. 1992 Direct simulation of particle dispersion in a decaying isotropic turbulence. *J. Fluid Mech.* **242**, 655–700.

Elghobashi, S. & Truesdell, J. C. 1993 On the two-way interaction between homogeneous turbulence and dispersed solid particles. I: Turbulence modification. *Phys. Fluids* A **5**, 1790–1801.

Eswaran, E. & Pope, S. B. 1988 An examination of forcing in direct numerical simulations of turbulence. *Comput. Fluids* **16**, 257–278.

Fessler, J. R., Kulick, J. D. & Eaton, J. K. 1994 Preferential concentration of heavy particles in a turbulent channel flow. *Phys. Fluids* A **6**, 3742–3749.

Hocking, L. M. & Jonas, P. R. 1970 The collision efficiency of small drops. *Q. J. R. Met. Soc.* **96**, 722–729.

Jonas, P. R. & Goldsmith, P. 1972 The collection efficiencies of small droplets falling through a sheared air flow. *J. Fluid Mech.* **52**, 593–608.

Kallio, G. A. & Reeks, M. W. 1989 A numerical simulation of particle deposition in turbulent boundary layers. *Intl J. Multiphase Flow* **15**, 433.

Maxey, M. R. 1987 The gravitational settling of aerosol particles in homogeneous turbulence and random flow fields. *J. Fluid Mech.* **174**, 441–465.

Maxey, M. R. & Riley, J. J. 1983 Equation of motion for a small rigid sphere in a nonuniform flow. *Phys. Fluids* **26**, 883–889.

McLaughlin, J. B. 1989 Aerosol particle deposition in numerically simulated channel flow. *Phys. Fluids* A **1**, 1211–1224.

McQuarrie, D. A. 1975 *Statistical Mechanics*. Harper & Row.

Patterson, G. S. & Orszag, S. A. 1972 *Numerical Simulation of Turbulence*. Springer

Pearson, H. J., Valioulis, I. A. & List, E. J. 1984 Monte Carlo simulation of coagulation in discrete particle-size distributions. Part 1. Brownian motion and fluid shearing. *J. Fluid Mech.* **143**, 367–385.

Riley, J. J. & Paterson, G. S. 1974 Diffusion experiments with numerically integrated isotropic turbulence. *Phys. Fluids* **17**, 292–297.

Saffman, P. G. & Turner, J. S. 1956 On the collision of drops in turbulent clouds. *J. Fluid Mech.* **1**, 16–30.

Smoluchowski, M. von 1917 Versuch einer mathematischen Theorie der Koagulationskinetik kolloider Lösungen. *Z. Phys. Chem.* **92**, 129.

Squires, K. D. & Eaton, J. K. 1990 Particle response and turbulence modification in isotropic turbulence. *Phys. Fluids* A **2**, 1191–1203.

Squires, K. D. & Eaton, J. K. 1991 Preferential concentration of particles by turbulence. *Phys. Fluids* A **3**, 1169–1178.

Sundaram, S. & Collins, L. R. 1994*a* Spectrum of density fluctuations in a particle-fluid system - I. Monodisperse spheres. *Intl J. Multiphase Flow* **20**, 1021–1037.

Sundaram, S. & Collins, L. R. 1994*b* Spectrum of density fluctuations in a particle-fluid system - II. Polydisperse spheres. *Intl J. Multiphase Flow* **20**, 1039–1052.

Sundaram, S. & Collins, L. R. 1996 Numerical considerations in simulating a turbulent suspension of finite-volume particles. *J. Comput. Phys.* **124**, 337–350.

Sundaram, S. & Collins, L. R. 1997 Collision statistics in an isotropic, particle-laden, turbulent suspension. Part 2. Model (in preparation).

Sundararajakumar, R. R. & Koch, D. L. 1996 Non-continuum lubrication flows between particles colliding in a gas. *J. Fluid Mech.* **313**, 283–308.

Vincent, A. & Meneguzzi, M. 1991 The spatial structure and statistical properties of homogeneous turbulence. *J. Fluid Mech.* **225**, 1–20.

WANG, L. P. & MAXEY, M. R. 1993 Settling velocity and concentration distribution of heavy particles in homogeneous isotropic turbulence. *J. Fluid Mech.* **256**, 27–68.

WANG, H., ZINCHENKO, A. Z. & DAVIS, R. H. 1994 The collision rate of small drops in linear flow fields. *J. Fluid Mech.* **265**, 161–188.

WEN, C. S. & BATCHELOR, G. K. 1985 The rate of coagulation in a dilute suspension of small particles. *Scientia Sinica* **28**, 172–184.

WERTHEIM, M. S. 1963 Exact solution of the Percus-Yevick integral equation for hard spheres *Phys. Rev. Lett*. **10**, 321–323.

YEUNG, P. K. & POPE, S. B. 1988 An algorithm for tracking fluid particles in numerical simulations of homogeneous turbulence. *J. Comput. Phys.* **79**, 373–416.

ZEICHNER, G. R. & SCHOWALTER, W. 1977 Use of trajectory analysis to study stability of colloidal dispersions in flow fields. *AIChE J.* **23** , 243–254.